NTNU

Norwegian University of
Science and Technology

Visualization of condensation over micro-structured surfaces

Raul Ciria Aylagas

Master of Energy and Environmental Engineering
Submission date: July 2016
Supervisor: Maria Fernandino, EPT

Norwegian University of Science and Technology
Department of Energy and Process Engineering

NTNU
Norwegian University
of Science and Technology

Department of Energy
and Process Engineering

EPT-M-2016- 174

MASTER THESIS

for

Student
Raul Ciria Aylagas

Spring 2016

Visualization of condensation over micro-structured surfaces

Background and objective

Efficient condensation of water vapour is required in several applications such as water harvesting, water desalination systems and thermal management systems in the process industry. In terms of heat transfer capabilities, dropwise condensation (DWC) is the preferred condensation mode as compared with the lower efficiency obtained from filmwise condensation. Maintaining a condenser surface under DWC conditions is one of the main challenges. With the latest advances in micro- and nano-technology, it is now possible to modify the surface structure and its wetting properties and try to promote dropwise condensation.

The goal of this project will be to visualize condensation on different structured surfaces and compare the effect of different surface structures.

The following tasks are to be considered:

1. Literature review on dropwise condensation and micro-structured surfaces for promoting this regime.
2. Fabrication of different micro-structured surfaces at the NTNU NanoLab. Characterization of the wetting properties of the surfaces by contact angle measurements.
3. Building of an experimental setup for visualization of condensation on the fabricated surfaces.
4. Visualization of condensation on the surfaces and comparison of the effect of the different structures on the condensation mode and wetting properties of the surfaces.

Within 14 days of receiving the written text on the master thesis, the candidate shall submit a research plan for his project to the department.

When the thesis is evaluated, emphasis is put on processing of the results, and that they are presented in tabular and/or graphic form in a clear manner, and that they are analyzed carefully.

The thesis should be formulated as a research report with summary both in English and Norwegian, conclusion, literature references, table of contents etc. During the preparation of the text, the candidate should make an effort to produce a well-structured and easily readable report. In order to ease the evaluation of the thesis, it is important that the cross-references are correct. In the making of the report, strong emphasis should be placed on both a thorough discussion of the results and an orderly presentation.

The candidate is requested to initiate and keep close contact with his/her academic supervisor(s) throughout the working period. The candidate must follow the rules and regulations of NTNU as well as passive directions given by the Department of Energy and Process Engineering.

Risk assessment of the candidate's work shall be carried out according to the department's procedures. The risk assessment must be documented and included as part of the final report. Events related to the candidate's work adversely affecting the health, safety or security, must be documented and included as part of the final report. If the documentation on risk assessment represents a large number of pages, the full version is to be submitted electronically to the supervisor and an excerpt is included in the report.

Pursuant to "Regulations concerning the supplementary provisions to the technology study program/Master of Science" at NTNU §20, the Department reserves the permission to utilize all the results and data for teaching and research purposes as well as in future publications.

The final report is to be submitted digitally in DAIM. An executive summary of the thesis including title, student's name, supervisor's name, year, department name, and NTNU's logo and name, shall be submitted to the department as a separate pdf file. Based on an agreement with the supervisor, the final report and other material and documents may be given to the supervisor in digital format.

☒ Work to be done in lab (Thermal engineering lab)
☐ Field work

Department of Energy and Process Engineering, 13. January 2016

Olav Bolland
Department Head

Maria Fernandino
Academic Supervisor

Research Advisor: Carlos A. Dorao

Acknowledgement

I would like to acknowledge all the people who have made this thesis possible. First of all my supervisors: prof. Maria Fernandino and prof. Carlos Alberto Dorao, who helped me a lot in the research and the experimental parts of this work. Also thanks to the PhD candidate Il-Woong Park who helped me in the designing and ordering of the photomask and with the cryoetching process. Special mention to Eivind Groestad and all the NTNU NanoLab staff, because he had the patience to teach me the working process in the cleanroom. Thanks also to Ximena de Diego for her help with their previous work in dropwise condensation. And finally thanks to Esther Lagunas Caballero who helped me with the revision and supervision of this document.

Summary

Water condensation is an ubiquitous phenomenon that happens widely in nature. It is also used in industrial applications such as water harvesting, desalination systems, thermal management and power generation. Filmwise condensation is commonly found in nature, but dropwise condensation is preferred due to the higher heat and mass transfer coefficients and lower thermal resistance. However dropwise condensation is difficult to obtain and sustain, so micro- and nano-structured surfaces have been studied as the most promising way to achieve it. Bio-inspired surfaces designed by mimicking natural surface structures have achieved a high degree of superhydrophobicity and some extraordinary characteristics such as self-cleaning and low adhesion. However, it has been discovered that the dropwise condensation process in superhydrophobic surfaces has some disadvantages, including the reduction of heat transfer performance during nucleation and growing stages and the low durability.

One of the most important steps of dropwise condensation is the droplet removal before the flooding of the surface. Self induced out of plane jumping has been studied several times in the past decades, but when the condensation process is running, it seems to be too slow to regenerate the surfaces and remove efficiently the droplets. Some additional mechanisms have been considered to enhance this process such as the electric field improvement of the droplet removal. Furthermore a new promising mechanism has been reported recently.

The sweeping droplet removal mechanism has proved to be faster than the jumping droplet removal mechanism, but there is not enough experience or evidence on this topic.

The main objectives of this thesis are to design and fabricate different microstructured surfaces for promoting dropwise condensation, enhancing the heat transfer performance, and the design and fabrication of an experimental setup for the visualization of the condensation process.

Fabrication of micropillars procedure has been learned and improved in order to achieve maximum quality on them. The process consists of two steps of photolithography and dry etching using the photoresist SU8. The etching process with ICP-RIE Cryo is a very delicate step where some adjust has to be done to the parameters depending on the kind of pillars that we want to obtain.

The visualization of the condensation process under laboratory conditions was achieved in a proper way except for samples with dimensions lower than 10μm. However dropwise condensation was not sustained and droplet removal has not been visualized anywhere. Another setup which allows more controlled conditions has been designed and made for further experiments of visualization of the condensation process and even roughly measuring the heat transfer performance.

Contents

Acknowledgement i
Summary iii
Contents v
Figures vii
Tables ix
1. Introduction 1
1.2 Background and motivation 1
1.2 Objectives 2
1.3 Scope of the work: 3
2 Theory Background 5
2.1 Structure definition 5
2.2 Wetting phenomena 7
2.2.1 Contact angle 7
2.2.2 Contact Angle Hysteresis 7
2.2.3 Surface classification 8
2.2.4 Droplet Morphology 9
3. Condensation 11
3.1 Dropwise condensation theory 11
3.3 DWC History and methods 14
3.3.1 Superhydrophobicity 14
3.3.2 Hierarchical structures 15
3.3.3 Surface funcionalization techniques 16
3.3.4 Amphiphilic surfaces 16
3.3.5 Droplet removal 18
4. Fabrication and characterization of micropillars 21
4.1 Material 21
4.2 Photomask 21
4.3 Fabrication Process 22
4.3.1 Cleaning 22
4.3.2 Dehydratation 22
4.3.3 Plasma Cleaning 23
4.3.4 Photoresist Spin Coating 23
4.3.5 Pre exposure soft baking 24

4.3.6 UV Exposure 24
4.3.7 Post exposure bake 24
4.3.8 Development 25
4.3.9 Dehydratation 25
4.3.10 Etching 25
4.3.11 Characterization 27
4.3.12 Resist removal 27
4.3.13 Cutting the wafer 27
4.3.14 Cleaning 29
4.3.15 Contact angle measurements 29
4.4 Design and characterization 30
5. Experimental setup for condensate droplets visualization 35
5.1 Visualization techniques review 35
5.2 Experimental setup design 35
5.3 Results 39
5.3.1 Cylindrical pillars 39
5.3.2 Square pillars 46
5.3.3 Discussion 48
6 Conclusion 51
6.1 Summary and conclusions 51
6.2 Recommendations for further work 52
Appendix A: Recipes 53
A.1 Recipe for micro pillar fabrication in 4” wafer 53
A.2 ICP-RIE Cryo Recipe 54
A.2.1 Recipe for cylindrical pillars 54
A.2.2 Recipe for square pillars 55
A.2.3 ICP-RIE Ctyo O2 Cleaning Recipe 56
A.3 Breaking Parameters 57
Bibliography 59

Figures

Figure 1 – Pillars structure, a) square pillars b) cylindrical pillars 5
Figure 2 – Contact angle of a droplet as the equilibrium between the different phase's surface tensions at their respective boundary 7
Figure 3 – Methods to measure the dynamic contact angles, on the left the volume changing method, on the right the tilting cradle method 8
Figure 4 – Surface classification by their contact angle 9
Figure 5 – Droplet morphologies 10
Figure 6 – a) Filmwise condensation sketch and thermal resistances diagram; b) Dropwise condensation sketch and thermal resistances diagram 12
Figure 7 – Ideal sketch of a hierarchical structure with H>>h and D>>d (29) 15
Figure 8 – Amphiphilic structure with hydrophilic tops and hydrophobic valleys allowing nucleation density control (36) 17
Figure 9 – Amphiphilic structure with hydrophobic tops and hydrophilic valleys allowing long-range coalescence and surface rejuvenation (37) 18
Figure 10 – Spontaneous jumping droplet phenomena (41) 19
Figure 11 – Sketch of the in plane self induced coalescence droplet removal, or sweeping droplet removal (9) 20
Figure 12 – Photomasks used to fabricate the micropillars. Squares in the left, circles in the right side 22
Figure 13 – Cleaning setup with acetone, ethanol, isopropanol and deionized water. 22
Figure 14 – Plasma cleaner front board 23
Figure 15 – Photoresist spinner with the SU8-5 ready to be deposited in the wafer. 23
Figure 16 – Mask Aligner MA6 with the mask and the wafer unloaded. 24
Figure 17 – Setup for developing process 25
Figure 18 – Diagram of the ICP-RIE chamber, power sources, wafer stage and temperature control system 26
Figure 19 – Rings used to make the plain adhesive surface in the left side and the scriber and breaker machine in the right side 28
Figure 20 – Broken samples in the left side and well cut samples in the right side 28
Figure 21 – OneAttensio Theta tensiometer with the syringe, the stage and the camera 29
Figure 22 - Cylindrical micropillars SEM imaging a) P=10, b) P=60 31
Figure 23 – Square shaped micropillars with W=10. They show different shape depending on the pitch a) P= 10 b) P=60 32
Figure 24 – Square shaped pillars with W=20. A) P=20, B) P=100 32
Figure 25 – Images taken during contact angle measurements showing the high contrast between the cylindrical pillars up (C1,C3, C4 respectively) and the square pillars down (SQ9 and SQ12 respectively). The images were taken from the computer screen with a camera. 34
Figure 26 – Photron Fastcam (Thorlabs) setup with the second disposition lenses. 36
Figure 27 – Samples stage and setup. Left: First setup with the green LED and the camera recording the side view. Right: Second setup with the mirror at 45° approximately to record the upside view and the optic fiber for the lighting. 37

Figure 28 – DC voltage source with the Thermo Electric Cooler connected to the middle source and the computer fan connected to the right source..... 37
Figure 29 – Condensation chamber design and instrumentation diagram design..... 38
Figure 30 – Condensation chamber setup and stage inside the chamber..... 38
Figure 31 – Side view and upside view of cylindrical micropillars with 5µm pitch..... 39
Figure 32 – Side view of pillars with pitch equal to 20 and 60µm 40
Figure 33 – Side view of condensation process in pillars with P=100µm 41
Figure 34 – Side view of condensation process in pillars with P=60µm 42
Figure 35 – Side view of condensation process in pillars with P=40µm 43
Figure 36 – Upside view of condensation process with P= 40µm 44
Figure 37 – Side view of condensation process in pillars with P=5µm 45
Figure 38 – Upside view of condensation process in pillars with P=5µm..... 45
Figure 39 – Upside view of condensation process in pillars with P= 60µm W=10µm 46
Figure 40 – Upside view of condensation process in pillars with P=10µm, W=10µm 47
Figure 41 – Upside view of condensation process in pillars with P= 100µm W=20µm 48

Tables

Table 1 – Wafers characteristics 21
Table 2 – Square pillars structure design characteristics 30
Table 3 – Cylindrical pillars structure, design characteristics 31
Table 4 – Cylindrical pillars structures, contact angle measurements. The value measured is the arithmetic average of the three measurements realized in different spot of the same sample 33
Table 5 – Square pillars structures, contact angle measurements. As the droplets occupy the whole sample only one measurement is made in every sample 33

Nomenclature

A_p	Projected surface
A_r	Real surface
A_t	Top surface
Θ_{cb}	Cassie-Baxter apparent contact angle
Θ_{cr}	Critical contact angle
Θ_e	Equilibrium contact angle
Θw	Wenzel apparent contact angle
CA	Contact Angle
CCP	Coupled Plasma Source
DI	Distiled
DWC	Dropwise condensation
ESEM	Environmental scanning electron microscope
ETEM	Environmental transmission electron microscope
FWC	Filmwise condensation
H	Height
ICP	Inductively coupled plasma
P	Pitch
PW	Partially wetting
RIE	Reactive ion etching
S	Suspended
Sccm	Standard cubic centimeters per minute
SEM	Scanning electron microscope

SSP	Single side Polished
W	Width
f	Contact surface fraction
r	Surface roughness

1. Introduction

1.2 Background and motivation

Vapor condensation on surfaces is a widespread phenomenon in nature and has a wide scope of application in industry. Understanding the governing mechanisms of water condensation can lead to an improvement in the efficiency of all the processes in which this phase change is involved producing a huge social and environmental impact.

As previously stated, water condensation has a wide range of applications. It is used in water harvesting (1), power generation (2), thermal management (3), water desalination (4) or environmental control (5). In fact, water condensation plays a crucial role in power generation. In this way, the thermal efficiency of the steam cycle is directly linked to the condensation heat transfer efficiency.

In addition to this, heating ventilating and air conditioning systems (HVAC) are affected by the process of condensation where an accumulation of water on thermal components can generate losses and therefore increases of costs (6) while these systems consume around 20% of the total power in developed countries.

In these systems, water condenses in a thin film rather than in small droplets, but since in 1930 dropwise condensation was discovered, it has attracted a lot of attention as its potential has been demonstrated in several studies. It has been proved that this mechanism can achieve up to an order of magnitude higher heat transfer coefficient than the filmwise condensation (7) (8). A lot of studies related to this topic have been carried out to date, most of them trying to achieve and sustain dropwise condensation. For this purpose, surfaces have been treated in order to change their chemical properties, their structure, and their roughness with more or less result.

These experiments involved in many cases to create a patterned pillar structure of only a few microns of dimensions. With these structures, the surfaces gain properties such as self-cleaning or anti-icing, which are very interesting from the point of view of the applications and have advantages for DWC.

The problem to sustain a continuous DWC is that the small droplets that are created in the surface have to be removed before they grow too much and thus they create a thin liquid film leading to filmwise condensation. In order to achieve this self sustained DWC, capillarity effects and surface energy have been used to make the droplets jump the surface when they coalesce with the neighboring droplets.

From this point some different structures with different properties have been used to achieve DWC and optimize it, but all of them were based on the out of surface jumping droplet mechanism which in some cases is too slow, so the DWC lead to FWC after some time.

Lately, a new mechanism of removal has been reported that can support the out of surface jumping droplet mechanism. It is based in the in plane droplet coalescence which leads to higher droplets departure velocities and that allows the departed droplet to coalesce with more droplets while it is travelling out of the surface (9).

However there are not enough experiments related with this mechanism to demonstrate that in practice, this is better than the traditional droplet jumping mechanism.

1.2 Objectives

The main objective of this work is to identify the different microstructured surfaces for enhancing condensation heat transfer as well as the techniques used to fabricate them, and develop a visualization setup to compare the condensation on different microstructured surfaces. The following sub-objectives are to be fulfilled:

1. Provide a review of the state-of-the-art in dropwise condensation on microstructured surfaces and their fabrication and identify remaining open questions and challenges in this field.
2. Fabrication and characterization of different microstructured surfaces in the NTNU NanoLab.
3. Design and build an experimental setup to visualize condensate droplets on the fabricated surfaces
4. Comparison between the different microstructures fabricated.

1.3 Scope of the work:

The scope of the review focuses on the mechanism of dropwise condensation on structured surfaces and the different designs of them to enhance some stages of the condensation process. Therefore, the understanding of the basic theory governing condensation in all these structures will be a priority.

The scope of the fabrication will be limited to one-tier-roughness structures, with cylindrical and square shaped pillars. The dimensions range will be 10-20µm for pillar width, 5-150µm for pillar pitch, and a thigh height range of 8-12µm as we want the height of all pillars to be ~10µm. The pillars are to be developed on 4" silicon wafers provided by NTNU NanoLab. Characterization will be made through SEM imaging and contact angle measurements.

The scope of the experimental setup design and building will be limited to the optic camera and lenses that we have in the EPT Lab. Additional materials used for the setup can be ordered such as a vapor chamber.

The scope of the comparison between the different microstructured surfaces is limited by the different droplet behavior during condensation that can be observed with the experimental setup built.

Structure

The structure of this project is made as follows:

- In Chapter 2 we introduce fundamental definitions and basic concepts for the further understanding of dropwise condensation and the different topics that are in this document.
- In Chapter 3 theory and experiments related to condensation on micro- and nano-structured surfaces are discussed.
- In Chapter 4 fabrication and characterization process of micropillars is described
- In Chapter 5 imaging techniques are discussed and the experimental setup designed and built is described. The results obtained with the experiments are discussed.
- In Chapter 6 we conclude this work and determine remaining challenges.

2 Theory Background

2.1 Structure definition

We are going to compare two different mechanisms of droplet removal, the out of plane self propelled droplet removal (or jumping removal) and the in plane self propelled droplet removal (or sweeping removal).

The first one has been attempted mostly with circular pillars, while the second mechanism has been reported recently and is based on the advantage of the corners of the square pillars.

Therefore we are going to fabricate and compare circular and square pillars. The structure of both kinds of pillars is defined in Figure 1:

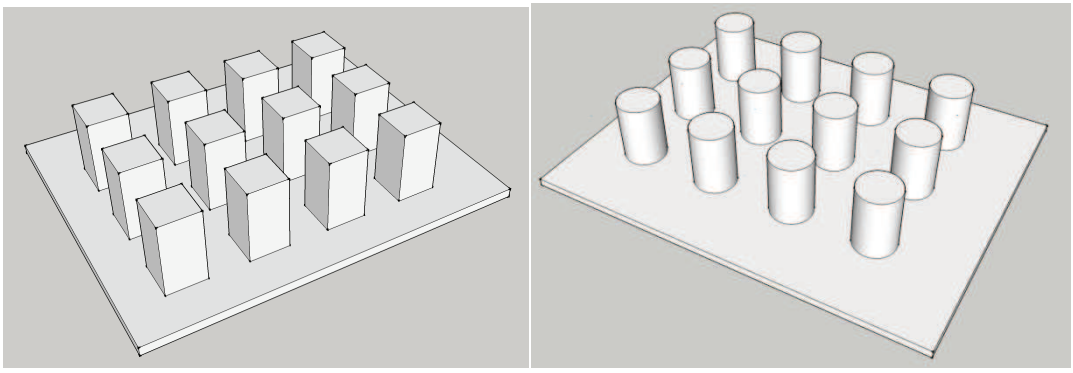

Figure 1 – Pillars structure, a) square pillars b) cylindrical pillars

To characterize the structures and know what properties they have it is fundamental to define two parameters, the surface roughness and the contact surface fraction. These are calculated using three different areas of our structure: the top surface area, the projected surface area and the real surface area. These areas depend on the geometry of the pillars, so they are different for the square and the circular shape:

In the case of the square pillars we have:

$$A_t = W^2 \qquad (1)$$

$$A_p = (W + P)^2 \qquad (2)$$

$$A_r = A_p + 4WH \qquad (3)$$

In the case of the circular pillars we have:

$$A_t = \frac{\pi W^2}{4} \qquad (4)$$

$$A_p = (W + P)^2 \qquad (5)$$

$$A_r = A_p + \pi W H \qquad (6)$$

With these areas we can calculate now the roughness ratio r and the contact surface fraction f:

$$f = \frac{A_t}{A_p} \qquad (7)$$

$$r = \frac{A_r}{A_p} \qquad (8)$$

2.2 Wetting phenomena

Wetting refers to the ability of a droplet to maintain contact with a surface; that is, to spread out and adhere when it is deposited in it. Wettability, the degree of wetting of a surface depends on the balance between adhesive and cohesive forces (10) . When a liquid is deposited on a surface it can wet the surface totally, it also can form a discrete droplet over the surface or it can have a behavior in the between, depending on surface energy. We usually use the contact angle to measure the wetting properties of a surface.

2.2.1 Contact angle

Young et al. first proposed that the contact angle θ of the droplets is determined by the equilibrium at the three phase contact line (11):

$$\cos\theta = \frac{\gamma_{sv}-\gamma_{sl}}{\gamma_{lv}} \qquad (9)$$

Where γ_{sl} , γ_{sv} and γ_{lv} are the solid-liquid, solid-vapor and liquid-vapor surface tensions, respectively. However the Young's equation assumes ideal solid surfaces, so it doesn't takes into account the contribution of roughness, surface chemistry, dissolutions or swelling.

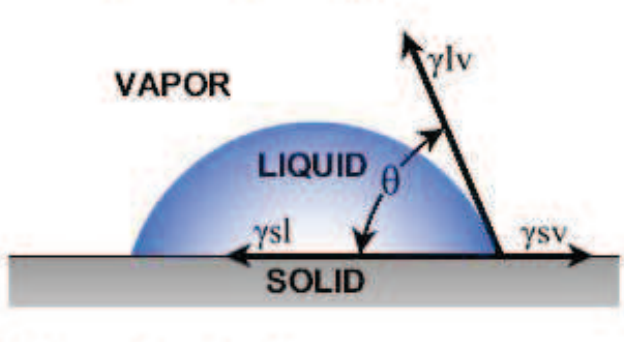

Figure 2 – Contact angle of a droplet as the equilibrium between the different phase's surface tensions at their respective boundary

2.2.2 Contact Angle Hysteresis

Contact angle hysteresis is the difference between the advancing contact angle and the receding contact angle. When we are measuring contact angles we notice that the contact angle can remain stationary if we don't disturb the liquid or dynamic if we interact with the liquid. We find that if a liquid has a determined contact angle, and we inject more liquid in it, the contact angle will increase, but the boundary between the three phases will remain stationary until it advances outward suddenly. Also, if we

reduce the amount of liquid, the contact angle recedes but the three phase boundary will remain in the same position until it recedes inward suddenly. The contact angle that we have just before the three phase boundary advances or recedes is what we call advancing contact angle and receding contact angle respectively.

$$\Delta\theta = \theta_a - \theta_r \qquad (10)$$

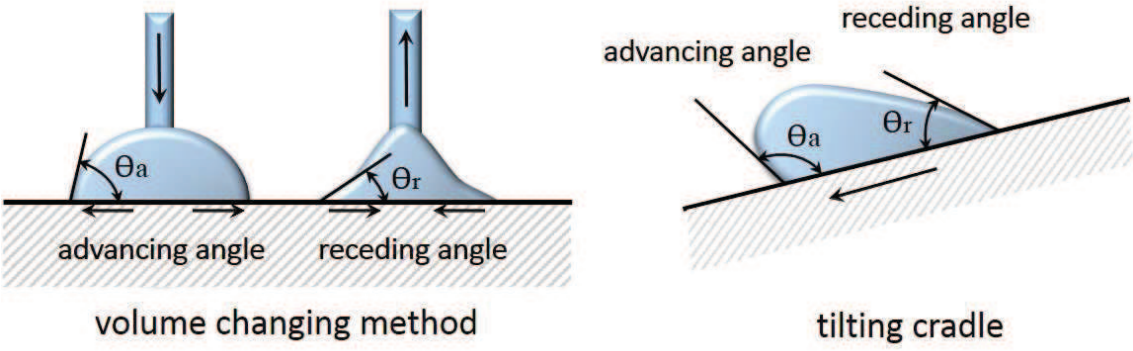

Figure 3 – Methods to measure the dynamic contact angles, on the left the volume changing method, on the right the tilting cradle method

Contact angle hysteresis is related with the droplet mobility. When a droplet is on a tilted surface, the static contact angles of the different limits of the surface start to change until the front and the back contact angles reach the advancing contact angle and the receding contact angle. After that happens, the three phase boundary starts to move, so the whole droplet will move downwards through the surface. The lower the contact angle is the higher mobility the droplets will have on the surface (12).

2.2.3 Surface classification

We can classify the surfaces depending on the contact angle. We have four main differentiations: Hydrophilic, hydrophobic, super hydrophilic and super hydrophobic.

In general we assume that when the contact angle is higher than 90 or 150 degrees, the surface is hydrophobic or super hydrophobic respectively, and it will repel water. While if the contact angle is lower than 90 or five degrees, the surface is hydrophilic or super hydrophilic respectively, and it will have affinity with water. We can observe experimentally that when a liquid is placed on a super hydrophobic surface the droplet will tend to form almost spherical droplets. In contrast, if we place a liquid in a super hydrophilic surface, it will tend to form a thin film over the surface.

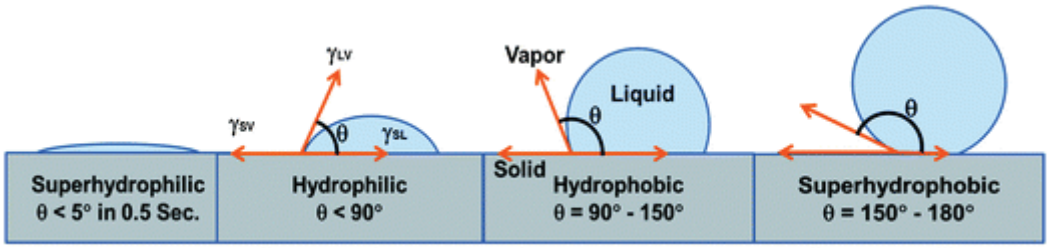

Figure 4 – Surface classification by their contact angle

2.2.4 Droplet Morphology

We have seen that by knowing the contact angle we can have some knowledge of the droplets behavior on a surface, however as we said before, the Young's equation assumes ideal solid surface and hereby it neglects some important properties of real surfaces and their consequences. Wenzel and Cassie continued the Young's work extending the wetting study to rough and porous surfaces. However they considered the droplets in different states of wetting in relation with the surface roughness.

In the Wenzel (13) state, the droplet completely wets all of the rough area, so there are no air bubbles between the liquid and the solid. In this state the Wenzel equation amplifies the contact angle by a factor r, where f is the surface roughness fraction:

$$\cos(\theta_W) = r\cos(\theta_e) \qquad (11)$$

Cassie and Baxter (14) developed another model considering that the droplet was in contact only with the tips of the roughness, so there was an air interface between some parts of the solid and the liquid. They showed that the contact angle in this case is defined by:

$$\cos\theta_C = f(\cos\theta_e + 1) - 1 \qquad (12)$$

These two droplet morphologies are named Wenzel and Cassie states respectively. We can see that in both cases, the roughness amplifies the chemistry characteristics of the surfaces. So if we have a hydrophobic flat surface, it will become more hydrophobic when roughness is added and if the flat surface is hydrophilic it will become more hydrophilic. In practice, it usually occurs that these models are not fully implemented, because the droplets don´t present any of both morphologies, instead, they are in a medium point between them.

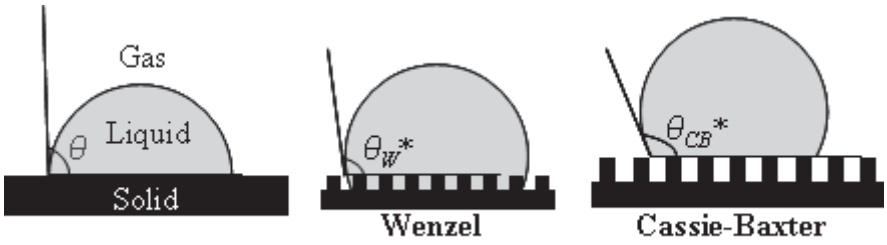

Figure 5 – Droplet morphologies

Even though both states can coexist in rough surfaces, Wenzel state is less desirable due to its higher adhesion to the surface compared to the Cassie state. Because of this, a lot of studies had focused on the Cassie state to achieve a very low adhesion in super hydrophobic surfaces leading to interesting properties such as self-cleaning or anti icing.

When a droplet is in the Cassie state, it can make a transition to a Wenzel state and vice versa. The limit between these two states is the so called critical contact angle (15) and can be obtained equalizing Wenzel and Cassie-Baxter equations

$$\cos\theta_{cr} = \frac{f-1}{r-f} \qquad (13)$$

The Cassie state is thermodynamically more stable when the physical contact angle θ_p (it is approximated with the static contact angle in a smooth surface) is bigger than the critical contact angle. The Wenzel state is more stable when the physical contact angle is smaller than the critical one.

3. Condensation

Condensation is a change of the state of matter from gas phase to liquid phase. This process occurs when the vapor temperature is reduced below the saturation temperature, and then the phase changes to liquid. Condensation starts with droplet nucleation in the phase in which the vapor is condensing, followed by droplet nucleus growth until it reaches a critical size. Depending on where these nucleus are formed, we can talk about homogeneous or heterogeneous condensation.

Homogeneous condensation occurs when the droplets nucleus are formed within a vapor phase, like a fog. Heterogeneous condensation occurs when the droplets are formed in contact with a substrate. The last one is the most interesting for us regarding real life applications in condensers. Consequently, from now on we are only going to study heterogeneous condensation.

Heterogeneous condensation occurs when the droplets are formed on a surface. However, as previously explained, there are surfaces with different properties. This implies that the droplets will be formed with very different morphologies. In general, we can difference between two modes of condensation: dropwise condensation (DWC) and film wise condensation (FWC).

3.1 Dropwise condensation theory

DWC is observed typically in hydrophobic or super hydrophobic surfaces and it consist on discrete droplets formed on the surface either in Wenzel or Cassie state or something in the between, while FWC usually occurs in hydrophilic or super hydrophilic surface. In FWC we can't see any discrete droplets, there is a film spreading on the surface. These two modes of condensation are not independent, on the grounds that almost every surface usually presents DWC at the first instants of the condensation process. However, while the droplets are growing and reaching higher sizes they can start to coalesce with the neighboring droplets, forming bigger ones and leading to FWC at the end.

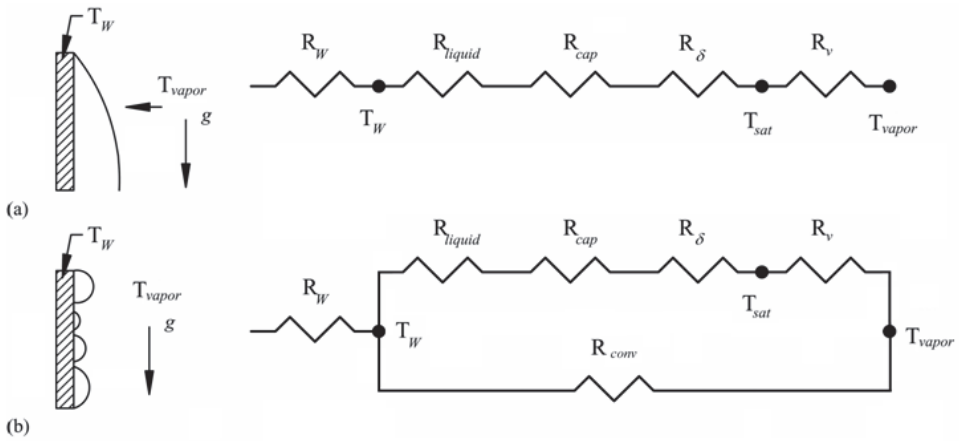

Figure 6 – a) Filmwise condensation sketch and thermal resistances diagram; b) Dropwise condensation sketch and thermal resistances diagram

DWC is more desired than FWC because it yields to a higher heat flux rate, and then efficiency improvement. This is because there is a higher amount of vapor phase in contact directly with the solid phase. As we can see in the figure 5 in FWC the liquid film adds more thermal resistance and consequently there is less heat flow moving from the vapor to the substrate.

The DWC mechanism has taken a lot of attention over the past decades since it was discovered in 1930 by Schmidt, Schuring, and Sellschoop (16) where they observed that the heat transfer coefficients were approximately 5-7 times higher in DWC than in FWC.

To understand the DWC mechanism we need to understand the processes that occur in it. As we said before, DWC starts with small discrete droplets forming along the surface which is called the nucleation process. If we take into consederation a rough surface, we notice that usually the droplets starts forming inside the roughness. Nevertheless we are going to consider roughness scales that are bigger that the magnitude of these first small droplets. Once that the first droplets are formed they start the growing process while at other parts of the surface where there are not nucleus some others start to appear.

As mentioned earlier, a liquid phase between the substrate and the vapor phase reduces the transmission of the heat, so the bigger the droplet grow, the slower it is going to be growing. At some point we will find that some big droplets will achieve dimensions similar to the roughness dimension and now there are some different morphologies or states that the droplets can show. As we introduced before in a rough surface the droplet

can be in a Wenzel state (W, wet) in a Cassie state (S, suspended) or in a state in the between (PW, partially wet).

These states are classified according to the kind of contact that the droplets have with the surface. In the point of view of the heat flux, we see that the W droplets are preferred when they are not too big because due to the high contact surface the droplet will grow bigger faster while the S droplets will grow slower. Miljkovik et al (17) showed that the droplet morphology on growth is an important factor to consider because in some cases, heat transfer performance is degraded due to the surface structures. They demonstrated that the growth of PW droplets is 6 times higher than in the S droplets and the heat transfer of individual droplets is from 4 to 6 times higher.

The next step is the process of departure. If we want to sustain DWC we need to remove the droplets that are formed to let new droplets nucleate and grow. We want to remove the droplets from the surface quickly to enhance heat transfer. If the droplets are not removed, they will start flooding the substrate leading to a FWC mode.

The droplets can be removed via gravity shedding, or with coalesce-induced droplet removal. Gravity shedding is too slow at these scales. Coalesce induced droplet removal has been studied recently since it was reported by Boreyko et al. (18)

This mechanism is based on the process that in some special cases occurs where two or more nucleuses coalesce on a surface. Depending on the characteristics of the surface, a bigger droplet formed very fast because of coalescence can lead to a high surface energy excess that will be dissipated via kinetic energy and then the droplet jump off the surface. The jumping is done usually on a direction almost perpendicular to the substrate, depending on the surface roughness and the droplets relative size. When the droplet jumps out of the plane of the substrate, we talk about jumping mechanism, if the droplet jumps in the same plane of the surface we talk about sweeping mechanism.

3.3 DWC History and methods

In 1930 Schmidt et al. identified the dropwise condensation mode. But the interesting thing was that they reported that heat transfer coefficients were between 5 and 7 times higher than those found during filmwise condensation. After that some successful attempts of industrial applications were demonstrated. The main problem was the difficulty of sustaining a long term dropwise condensation when used under industrial conditions; however Zhao et al. developed a successful application on a power plant condenser. After Zhao et al. there haven't been successful implementations on industrial conditions (19). But the last years, with the development of the idea of the amphiphilic surfaces some attempts of developing a cheap and robust surface that can promote surface condensation have been made (20).

3.3.1 Superhydrophobicity

Until the last decade, the majority of the techniques used to promote DWC try to enhance the superhydrophobicity of the surface. Superhydrophobity is usually achieved coating a microstructured surface. It was studied for the first time by Johnshon and Dettre in 1964 using rough hydrophobic surfaces (21).

Whit the findings related to the surface of lotus leaves, people have started exploring natural surfaces or bio-inspired designs to understand complex roughness and water repelling properties. The lotus leaves present complex micro- and nano-structures which creates the so called "lotus effect" or self-cleaning property (22). This phenomenon is based on the high mobility of the water droplets that roll of the surfaces carrying dirt and pathogenic organisms with them (23).

As the causes of self cleaning property are due to physical and chemical properties of the nano- and microstructures that are in the lotus leaves, the property can be created artificially mimicking those structures (24). However, the lotus leaf is not the only that has that self cleaning property, other kind of plants have been found to be superhydrophobic and present self cleaning (25). Taro leaves, Indian canna leaves or rice leaves are plants that show similar structures to the lotus leaf. But it is not only in plants; but also in animals that we can see some examples of superhydrophobic surfaces; for example in the legs of a water strider, or in the wings of some insects (26).

To sum up, some superhydrophobic surfaces have been found in nature, and one common characteristic is that all of them presented a hierarchical structure.

3.3.2 Hierarchical structures

A hierarchical structure consists of multiple roughness length scales, usually a micro patterned structure combined with a nanostructure on all the surfaces of the microstructures. This kind of structures usually leads to higher contact angles and lower contact angle hysteresis. Typically is stated that to consider a surface superhydrophobic, the contact angle should be more than 150º and the contact angle hysteresis should be lower than 5º. But despite a lot of the hierarchical structures studied presents superhydrophobicity, it don't necessarily happen. To ensure high contact angles, the materials used in the second tier roughness should have low surface energy, so different kinds of coatings are used on this purpose (27), (28).

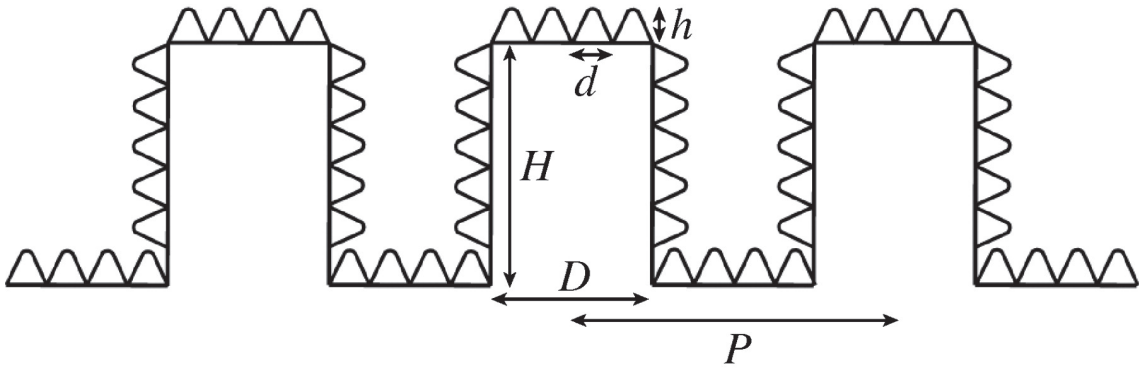

Figure 7 – Ideal sketch of a hierarchical structure with H>>h and D>>d (29)

One of the fundamental advantages of the hierarchical structures with two tier roughness regarding dropwise condensation is that we usually find the droplets on a suspended S state. This is both an advantage and a disadvantage because as we explained before, the heat transfer performance is decreased during the nucleation and growing stages, but the departure of the droplets is easier. As one of the main problems in DWC is the sustainability of the condensation mode it is more important to achieve the proper shedding of the droplets than the heat transfer performance during early droplet stages.

However in one tier (non-hierarchically) surfaces we can also find those S droplets, Nosonovsky and Bhushan demonstrated that hierarchical structures are essential to ensure stability during Cassie-Baxter suspended state (30).

3.3.3 Surface funcionalization techniques

The techniques used to lead a sustainable DWC mode have been studied over the past fifty decades. One of the first topics of interest was the application of non wetting surfaces with coatings allowing easy droplet removal. The different coatings studied had attracted a lot of attention since we can take advantage of their wetting properties without losing heat transfer performance because of their small thickness and their favorable application on heat transfer materials such as cooper, stainless steel, titanium or aluminum. The most studied coatings are self-assembled monolayers (SAMs), polymers, noble metals, ion implantation and rare earth oxides. Enright et al. (31) gives a very good review of all the advantages and disadvantages of these methods. However there are serious issues in their application and it is very difficult to achieve a good balance between durability, costs and performance.

- Self-assembled monolayers are thin molecular films that are formed spontaneously on the surface and usually have hydrophobic tails pointing outwards. As the film is very thin it doesn't make a significant contribution to the thermal resistance of the surface. Despite under laboratory conditions they can sustain DWC during 10 hours; after that the coating is progressively removed leading to flooding and filmwise regime.
- Polymers are also typically used to promote DWC however due to the need of high adhesion between the substrate and the polymer layer; thick layers are needed even when they increase the thermal resistance significantly. Plasma-enhanced chemical vapor deposition (PVD) is a promising technique which allows creating a very thin layer of polymer on the selected surfaces.
- Noble metals surfaces layers need physisorbed contaminants to promote DWC because when the surface is clean they give filmwise condensation regime.
- Ion Implantation has been demonstrated to sustain DWC under low sub cooling level conditions. However the cost of this technique is quite expensive and leads to filmwise condensation for high sub cooling levels.

3.3.4 Amphiphilic surfaces

Superhydrophobity shows a lot of advantages and is the kind of surface that we would want to have to promote dropwise condensation, but there are some issues regarding heat transfer performance during the nucleation and growth stage that need further

research and development. This development came while studying some insect skins in nature. Researchers found the Stenocara beetle which has a special back that allows him to obtain water in arid desert conditions by condensing the fog droplets (32), (33). His back is formed by a hydrophobic waxy structure with a random array of hydrophilic bumps. This hydrophilic region collects water when there is presence of fog in the air. The droplets formed in the hydrophilic grow until they cover the entire bump and when a big size is reached they start to roll over the back to the beetle's mouth by their own weight.

Some research has been made in order to mimic this amphiphilic structure in laboratory (34). The bio-inspired structure that usually is used consists on micro pillar arrays with hydrophilic tops and the rest of the surface is hydrophobic (35). The hydrophobic or hydrophilic regions are usually fabricated with coatings techniques.

Hou et al. (36) fabricated this hybrid structures and they reported a new condensation mode that they called recurrent filmwise and dropwise condensation. The process that they observed was that the hydrophilic regions are the firsts to have droplets on it and due to their wetting characteristics, filmwise condensation is observed on them. But when the liquid reaches the limit between the hydrophobic and the hydrophilic region the growth of the film starts to increase the contact angle of the film that starts to turn into a droplet. When the droplets grow enough, self-induced coalescence departure spontaneously happens. This structure combines the benefits of hydrophilic surfaces (fast nucleation, fast grow) and hydrophobic surfaces (transition to dropwise regime, self-induced coalescence droplet removal.

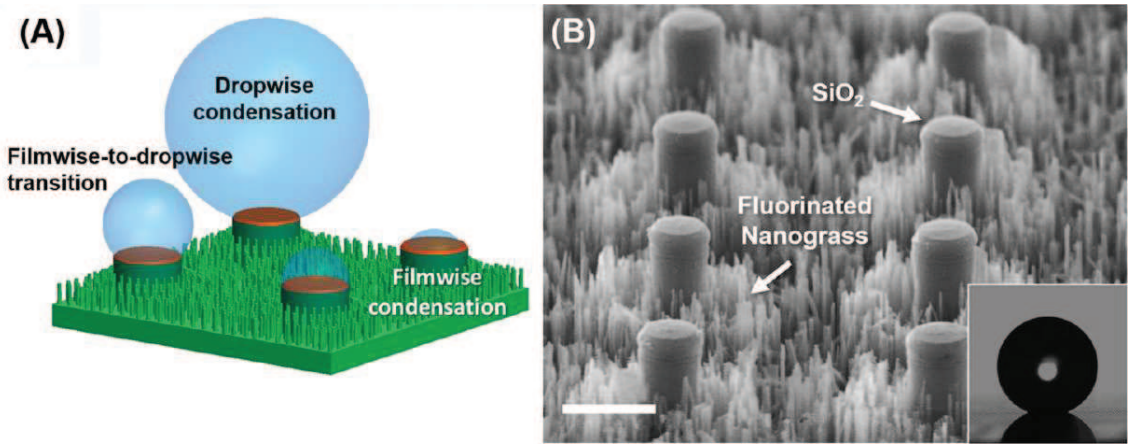

Figure 8 – Amphiphilic structure with hydrophilic tops and hydrophobic valleys allowing nucleation density control (36)

Amphiphilic structures with the inverse pattern, that is, hydrophobic pillar tops and hydrophilic valleys can be used also to enhance condensation. (37), (38), (39) In this case the process of condensation is different. In this surface the pillars have a very tight spacing and as only the top of the pillar is hydrophobic and the rest is hydrophilic there is a film of liquid between the pillars but the height of this film is the same than the height of the pillars. The top of the pillars are not wetted because of the hydrophobic coating. The water droplets that are formed over the top of the pillars are connected with the liquid film that fills the interspaces between the pillars if they are in the Wenzel state, but when they are in the Cassie state they are not connected with the liquid film. As the W droplets are connected by the liquid film coalescence occurs in via the liquid film when the pressures on them are different. This allows a surface regeneration and posterior nucleation enhancing heat and mass transfer during the nucleation and growth phases.

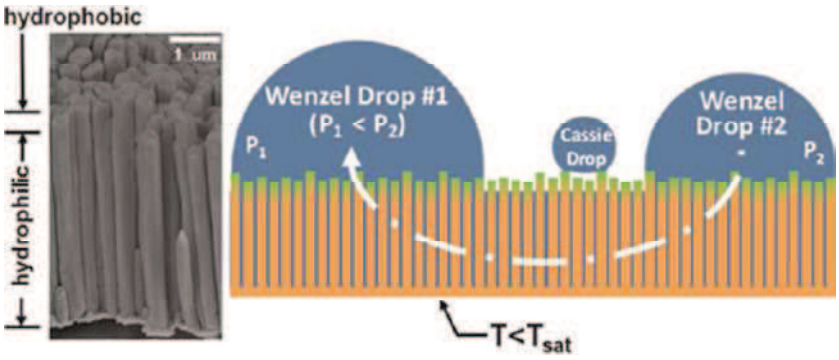

Figure 9 – Amphiphilic structure with hydrophobic tops and hydrophilic valleys allowing long- range coalescence and surface rejuvenation (37)

3.3.5 Droplet removal

The main characteristic of the dropwise regime is the removal of the droplets before they are so big that flood the surface. The sustaining of the dropwise condensation highly depends on this process, and if it is not well performed filmwise condensation will appear sooner or later.

The traditional gravity induced shedding is not efficient enough to remove all the droplets and need the diameter of the droplets to be at least 2.7 mm. This is why some alternatives to this droplet removal mechanism have been investigated.

The self-induced coalescence droplet removal has been a topic of high interest due to its potential to sustain dropwise condensation. This mechanism was discovered by Kollera and Grigull (40) in 1969 studying condensation of mercury in steel surfaces. After that some experiments demonstrated that this mechanism doesn't need any external force to remove the droplets (18).

The spontaneous motion is powered y the release of the excess of surface energy into kinetic energy. This phenomenon occurs when two or more droplets touch each other and then they coalesce, forming only one big droplet with a volume equal to the sum of the different droplets volume. The coalescing of the droplets is very fast and thus the droplets don't have enough time to change its state, so the surface energy is increased in a small instant. As a result of this excess of energy, the droplet jumps off the surface.

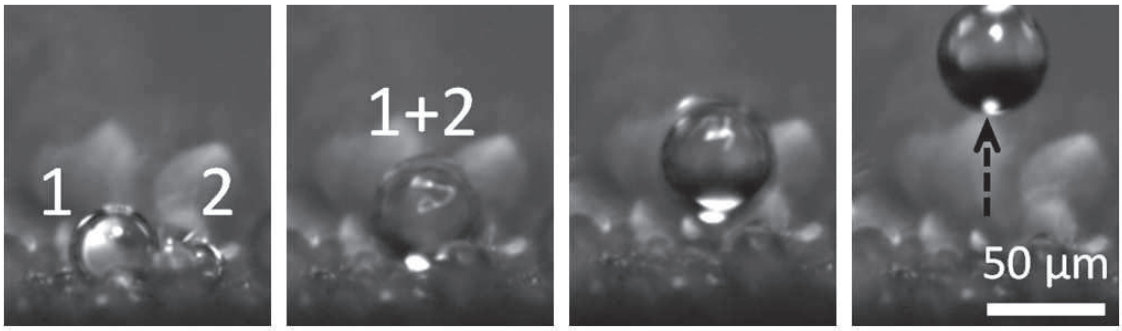

Figure 10 – Spontaneous jumping droplet phenomena (41)

To achieve droplet jumping of PW and S droplets it is important to have low solid fraction ($f<0.1$) or hierarchical structures. If the solid fraction is too large, PW and S droplets may not be possible to jump due to high adhesion (42).

Some studies have been made about the characteristics of the jumping process regarding the number of coalescing droplets and the speed of the resulting droplet. The results of these studies showed that the when more than two droplets coalesce the speed of the resulting droplet should be greater than the speed obtained when only two droplets are coalescing (43). But in practice some studies found that when more than two droplets coalesce the trajectory is not usually on the perpendicular of the surface due to asymmetries of volume and position between the droplets and the speed is reduced considerably (44). So the highest speed is achieved when two droplets coalesce.

The speed of jumping is an important parameter to take into account because if the speed is not high enough the droplets could return to the surface reducing the efficiency

of the droplet removal process and therefore the overall efficiency of the condensation process.

In order to prevent the droplets from returning to the surface, some researchers have used systems with electrostatic fields that take advantage of the positive charge that the jumping droplets have due to electric double layer charge separation at the hydrophobic coating/condensate interface (45) (46).

Another promising variant of this process is the in-plane self induced droplet removal. The principle under this mechanism is the same as in the jumping droplet but in this case the droplets part in a trajectory in the same plane of the surface. This was reported first by Boreyko et al. (9) and has not been studied deeply yet. In this process the droplets are situated between the pillars and they are in contact with the sidewalls of the pillars.

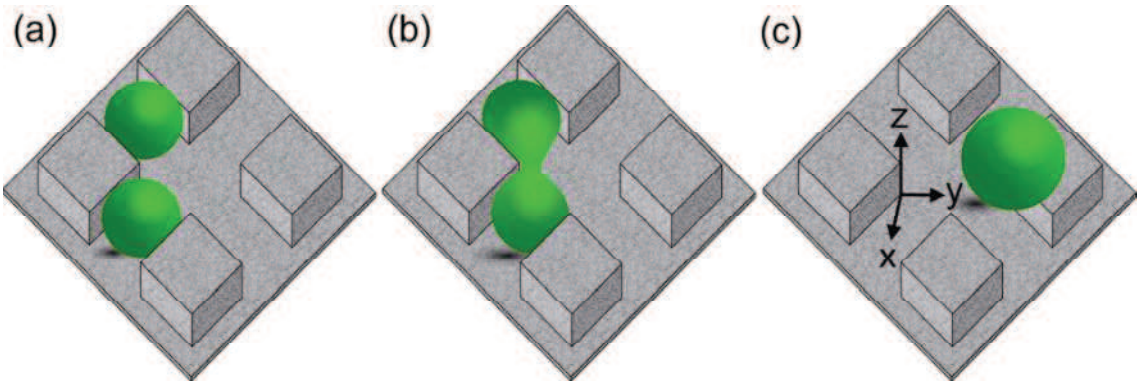

Figure 11 – Sketch of the in plane self induced coalescence droplet removal, or sweeping droplet removal (9)

When the coalescence is produced the droplets take a trajectory in the direction perpendicular to the surface in which they rest. In this case as they are pinned to the sidewalls of the pillars they leave with a direction in the same plane of the macroscopic surface. In his trajectory the droplet will merge with the other droplets that it encounters in its way, and after some coalescing process take place, the droplet will jump out of plane due to jumping process. This can provide a faster droplet removal as it can create a chain of coalescences and remove more droplets once one of them jumps. This is made trough square pillars because the corners that they have, favors the jumping as more surface energy is released and thus more velocity is reached.

.

4. Fabrication and characterization of micropillars

Now we are going to review the fabrication process of micropillars in silicon that we are going to perform in the laboratory to obtain the desired micro structure for the condensation experiments.

4.1 Material

Silicon is one of the most available elements on earth, and is easy to find in nature in the form of silica. It is cheap and has very good properties what makes it very used in different applications. NTNU Nano lab provides us Silicon wafers with the following characteristics:

Supplier	University Wafer
Diameter	4", 10.2 mm
Polish	SSP
Dopant	B
Fabrication method	Czochralski (CZ)
Thickness	500-550 µm
Orientation	⟨100⟩
Type	P
Resistivity	0-100
Test	Test

Table 1 – Wafers characteristics

4.2 Photomask

After proceeding with the microstructures fabrication we must have a photomask with the desired pattern on it. The photomask has to be designed with special software, in this case with CleWin 5. Then, it is printed on a thin film or a chrome glass, with 5µm resolution in the first case and 0.8µm in the second case. We prefer to use a chrome glass photomask due to the better resolution that will allow us to make well defined shapes in the structures. So we have designed a photomask with a square pattern and we have ordered it to Micro Lithography Services Ltd. We also are going to use a chrome glass photomask for the cylindrical pillars but we have one in the Department that was ordered by other students.

Figure 12 – Photomasks used to fabricate the micropillars. Squares in the left, circles in the right side

4.3 Fabrication Process

4.3.1 Cleaning

The first step in the process is cleaning the Si wafer so it is not contaminated to ensure good results. Even when we are working on a ISO 5 or 6 room, some items like the plastic carriers and the tweezers must be the cleanest as possible every time to minimize negative contributions during all the process.

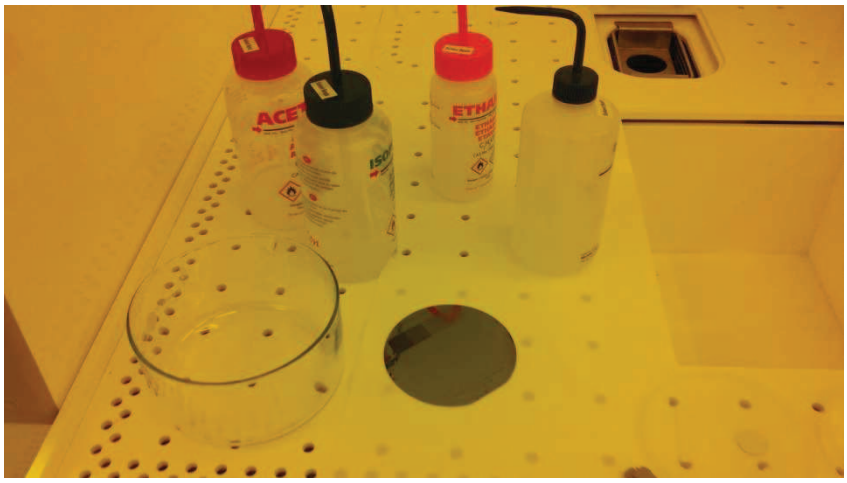

Figure 13 – Cleaning setup with acetone, ethanol, isopropanol and deionized water.

The wafer is cleaned by splashing the wafer with acetone until the whole wafer is covered. Then it is showered with ethanol, isopropanol(IPA) and deionized water. Instantly the wafer is dried with N2 until there are no droplets on the surface.

4.3.2 Dehydratation

We heat up the wafer in a hot plate at 200 C during 5 minutes. To ensure that the back of the wafer is not contaminated by other particles that can be in the hot plate, we use

our own clean silicon wafer. During this step all the OH bonds are thermally cracked promoting resist adhesion.

4.3.3 Plasma Cleaning

We use plasma cleaner (Femto, Diener Electronic) to remove all the organic contaminants in the surface via reaction with O2. With this step we also make the surface more hydrophilic and potentiate resist adhesion. We use these parameters: 50% O2 (50sccm), 50% power (50W).

Figure 14 – Plasma cleaner front board

4.3.4 Photoresist Spin Coating

SU 8-5 by MicroChem is used as negative photoresist, so the resist further exposed to UV light will not be removed after the photolithography process. A spin coater is used to create a thin layer of photoresist on the Si wafer. First the wafer is placed on the chuck of the spinner and when it is centered, vacuum is applied so the wafer can't leave the chuck. Then 4 ml of SU 8-5 are applied in the center of the wafer with a pipette continuously avoiding air bubbles with the last drops. The pipettes are not re-usable; once the resist is applied they have to be emptied and cleaned properly.

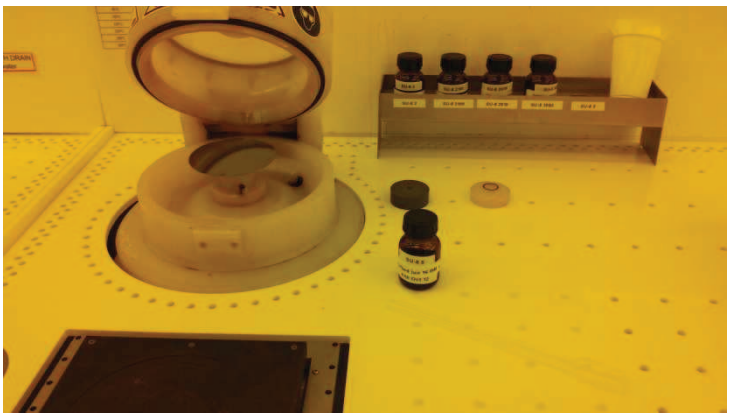

Figure 15 – Photoresist spinner with the SU8-5 ready to be deposited in the wafer.

There are three parameters to adjust on the spinner: time, speed and acceleration. Thickness of the resist layer is inversely proportional to all of them.

4.3.5 Pre exposure soft baking

When the photoresist layer is applied in the surface, it must be soft baked to evaporate the solvent and densify the layer. For this purpose two hot plates are set at 65 and 95 C. The wafer is left 1 minute in the first hot plate and then transported to the second plate during 3 minutes. Then the wafer is cooled down in a cool plate for 3 minutes.

4.3.6 UV Exposure

In this step the wafer is irradiated with UV light, in order to amplify the cross linking reaction. SU8-5 is a negative photoresist, thereby, the exposed regions correspond to the desired areas that we want to have on our substrate. The unexposed regions will be removed later during the development step.

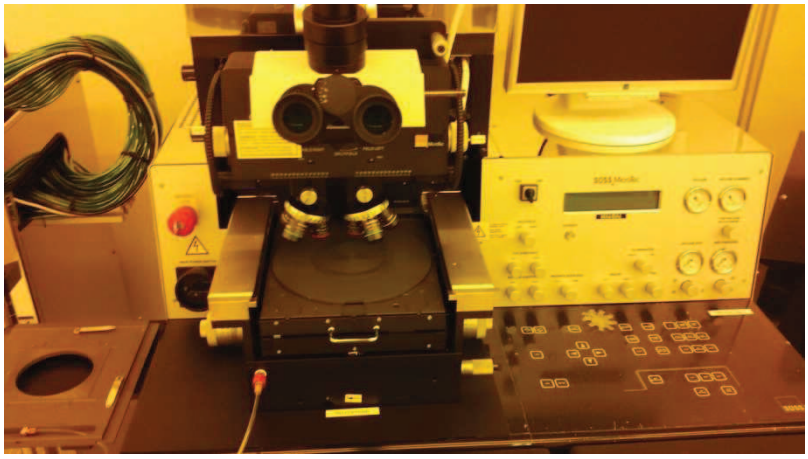

Figure 16 – Mask Aligner MA6 with the mask and the wafer unloaded.

A MA6 Mask aligner is used in this step. To obtain the desired cross linking property it's very important to irradiate the correct exposure dose. This is controlled measuring the intensity of the UV lamp with an optometer, and depending on it, we adjust a proper exposure time.

$$Exposure\ time = \frac{Exposure\ dose\ \ [mJ/cm^2]}{Lamp\ intensity\ [mW/cm^2]}$$

4.3.7 Post exposure bake

After the exposure it's necessary to perform a soft baking to cross-link the exposed areas on the layer. The wafer is therefore baked in a hot plate at 65 C for 1 minute and

then changed to another hot plate at 95 C for 2 minutes. Then the wafer is cooled down on a cold plate during 3 minutes.

4.3.8 Development

In this step, we remove the non-exposed areas that we don't want to be in our substrate. The developer mr-Dev 600 (Micro resist Technology GmbH) is used to fulfill that objective. We use two beakers, one with enough developer to immerse the wafer, and the other is under a tape, full of water and with the tape slightly open, having a laminar flow on the surface of the water going out of the wafer. The wafer is going to be immersed in the first beaker using a sift during 1 minute, and then in the second beaker during 30 seconds. After that it is immediately dried with N2. If there are some marks or oil observed, the process is repeated.

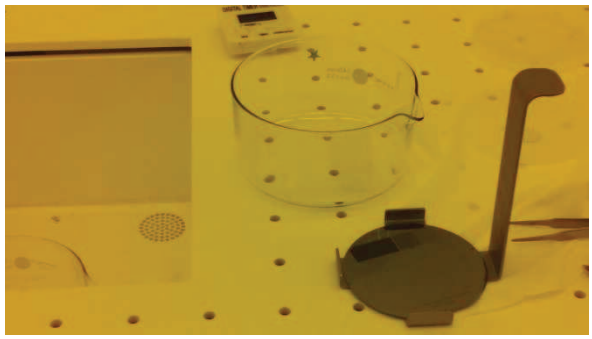

Figure 17 – Setup for developing process

4.3.9 Dehydratation

We heat up the wafer in a hot plate at 200 C during 5 minutes. To ensure that the back of the wafer is not contaminated by other particles that can be in the hot plate, we use our own clean silicon wafer. This step is important to make the etching process more reliable.

4.3.10 Etching

There are two options of etching silicon, dry etching and wet etching.

In the wet etching process, silicon is etched in an aqueous solution where the exposed parts of the photo resist are removed. However there are some issues to solve on this option such as anisotropy or the use of hazardous substances like HF.

In the dry etching process, silicon is etched using gaseous etchants. This is the method which we are going to use in this project. This is usually performed via Reactive Ion Etching (RIE) where plasma with a combination of gases strikes the surface of the wafer

reacting with the atoms in the upper layers. The cost common processes used in dry etching are the Bosch process and the cryoetching process.

The first operates at ambient temperature and uses SF6 etching steps alternated with c-C_4F_8 pasivation steps. However fast response mass flow controllers are required for high etch rates and this equipment is not available at the NTNU NanoLab.

Cryoetching is performed at -120°C and uses SF_6 and O_2 as described by d'Agostino et al. Smooth sidewalls can be obtained using this process and that is what makes it preferable. We are going to use an inductively coupled plasma reactive ion etcher, ICP-RIE Cryo (Plasmalab 100- ICP180, Oxford Instruments) with AlO_2 dome, wafer carrier and clamp. The ICP-RIE uses two independent RF sources, one to strike plasma in a gas mixture and one to create a DC bias which extracts and accelerates ions and radicals from the plasma towards a sample surface. This gives independent control of ion density and energy

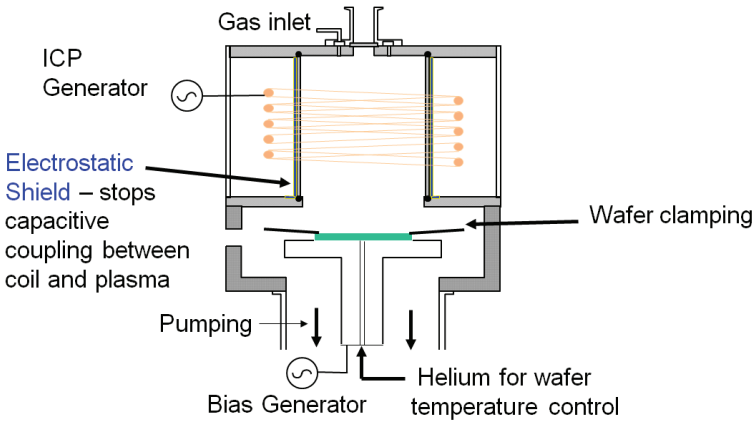

Figure 18 – Diagram of the ICP-RIE chamber, power sources, wafer stage and temperature control system

The cryoetching process is very sensitive to wafer temperature, so liquid nitrogen must be used to cold the backside of the wafer while helium is used to control temperature of the wafer due to its good conductivity. The etching time will depend on the height that we want to have in the pillars. Some previous studies made by other students in the EPT department showed the different defects that we can find after the etching process and developed a recipe and some advices to avoid them. With this information we are able to etch good quality cylindrical pillars, however it doesn't works so good to define the corners of the square pillars. Therefore some experiments have been made with reduced

oxygen percentage in the mix of gases. After some experiments a good proportion was found and corners were well defined.

4.3.11 Characterization

Once the sample is produced, we need to characterize the structures fabricated and check if some errors were made during the process followed with further improvement of it. The Characterization is done with a Scanning Electron Microscope (JEOL SEM) under high vacuum conditions. The sample must be placed in the holder with some adhesive tape to ensure that it's not falling. Here we are going to control that the sample has not defects after the etching process. We can also measure the height obtained, but is recommendable to measure it again after the removal of the photo resist in the case that we want it. To make this we select a tilting angle of 30 degrees because of the easy trigonometric operation to measure heights. It is very important that the wafer don't crash in the detector, so we have to select a distance of Z=18mm.

4.3.12 Resist removal

After the etching process is usual to find that some of the resist has not been etched. In some cases we want to remove it because the top of the pillars will have different properties depending on the chemistry of the surface on it. The contact angle of SU8-5 is 73° but after the etching process, the resist can have some nano roughness that will give to the top of the pillars extra hydrophobicity having a coating-like effect (47). The cleaning process is done via Reactive Ion Etching but using only O_2 during 30 minutes.

4.3.13 Cutting the wafer

For our experimental setup we are going to test each one of the samples separately, not the whole wafer at a time. The breaking process is done in the DLX3 scriber and breaker machine. In this step, a diamond tip scribe lines on the wafer with the separation that we select, between the different samples in the wafer. After that the wafer is moved under an anvil which makes pressure over the wafer while a thing hits the back of the wafer in the same plane where the line was scribed, leading to a clean cut of the wafer in a straight line. This process is very delicate because the wafer can easily break in

pieces if we don't select the appropriate parameters, and therefore the samples will be destroyed and we must discard them.

Figure 19 – Rings used to make the plain adhesive surface in the left side and the scriber and breaker machine in the right side

At first we need to make a very flat surface with adhesive plastic using two hoops and some plastic covers as shown in the picture. When the small grey hoop is into the blue big hoop, we put out the plastic covers and cut the rest of the adhesive blue plastic that isn't in the rings. After that we put the wafer on the center of the plastic and the whole thing on the vacuum chuck. Then we select the appropriate recipe and parameters that can be found in appendix C and we run auto scribe and beak process. Some alignment and first street selection has to be done and then the machine starts scribing and breaking the wafer. At the end of the process we should have the samples of approximately 16.5 mm separately. If something goes wrong and some of them are not broken we can do it manually being very careful not to damage the microstructure.

Figure 20 – Broken samples in the left side and well cut samples in the right side

4.3.14 Cleaning

After the breaking process some dust and silicon particles are dispersed along the samples, so it is necessary to clean the samples. We use solvents as ethanol and then dry with N_2.

4.3.15 Contact angle measurements

Contact angle is measured using the tensiometer OneAttensio Thetha. It is an optical computer controlled and programmable tensiometer formed by a video camera, a LED light and a sample stage. Sessile drop is the method that we used to do the measurements. When a droplet is placed on the sample stage the video camera records it and the image is sent to a computer that, with the convenient software analyzes the image that it is receiving.

Figure 21 – OneAttensio Theta tensiometer with the syringe, the stage and the camera.

The models used for the analysis can be Young-Laplace method, circle method, conic section method and polynomial method. Young-Laplace method has been used to do the measurements.

Before using the tensiometer, we need to calibrate it, in order to achieve good precision on the measurements. The syringe that is going to be used must be filled up with distilled water and the needle should be carefully cleaned. A crystal syringe as the one in the picture is used.

Both static and dynamic angles can be measured. To measure static contact angles we only need to place a droplet on the sample surface and record it with the computer. The duration of the recording is a maximum of approximately 10 seconds. When the record is done, the software analyzes the images and gives the contact angles over time and other measurements as the baseline length or the droplet volume. To avoid errors in the measurement due to the size of the droplet is recommended to use a droplet that is 3 or 4 times the needle diameter. And also placing the needle in height where it doesn't touch the droplet but it's not too far from it.

In order to measure dynamic contact angles, after placing a droplet in the sample surface we need to add more water volume or quit water volume depending on the

contact angle that we are measuring, advancing or receding. For advancing contact angle we have to add water slowly while we record and we will see that the contact angle increases until the baseline grows. The angle just before that moment is the advancing contact angle. With the receding contact angle we apply the same method but inverse way, we quit extract water from the droplet until the baseline is reduced, and then we can know the receding contact angle.

4.4 Design and characterization

We are going to experiment with square micropillars with one tier roughness. We want to test if the sweeping removal actually happens in non hierarchical structures. To avoid the effect of the coating of the rest of the SU-8 that is not etched in the etching process, we are going to remove it of the square pillars. This is because the droplet removal in which we are interested relies on the chain of coalescences that take place due to the corners of the pillars. We are going to experiment with pillars with a large range of pitches, and only two values of H/W. The value selected for the height and width of the pillars is 10µm as it is recommended in previous works (9). The mask that we have designed has the following sequences of square pillars:

Sample ID	W (µm)	H (µm)	P (µm)	r	f	θ_{crit} (◦)
SQ1	10	10	5	2,778	0,444	103,8
SQ2	10	10	10	2,000	0,250	115,4
SQ3	10	10	20	1,444	0,111	131,8
SQ4	10	10	30	1,250	0,063	142,1
SQ5	10	10	40	1,160	0,040	149,0
SQ6	10	10	50	1,111	0,028	153,8
SQ7	10	10	60	1,082	0,020	157,4
SQ8	10	10	70	1,063	0,016	160,1
SQ9	20	10	10	1,889	0,444	112,6
SQ10	20	10	20	1,500	0,250	126,9
SQ11	20	10	40	1,222	0,111	143,1
SQ12	20	10	60	1,125	0,063	151,9
SQ13	20	10	80	1,080	0,040	157,4
SQ14	20	10	100	1,056	0,028	161,1
SQ15	20	10	120	1,041	0,020	163,7
SQ16	20	10	140	1,031	0,016	165,7

Table 2 – Square pillars structure design characteristics

As we can see we are going to use two different widths for the square pillars, with the mask that we designed. But we cannot do it with the cylindrical pillars because the mask that we had in the department only had one width of pillars corresponding to 10µm. In the case of the cylindrical pillars, we are not going to remove the SU8 of the top of the pillars because it will give extra hydrophobicity, and the effectiveness of the jumping droplet mechanism relies in this characteristic. The circular samples are the following:

Sample ID	W (µm)	H (µm)	P (µm)	r	f	θ_{crit} (◦)
C1	10	10	5	2,396	0,349	108,5
C2	10	10	10	1,785	0,196	120,4
C3	10	10	20	1,349	0,087	136,3
C4	10	10	30	1,196	0,049	146,0
C5	10	10	40	1,126	0,031	152,3
C6	10	10	50	1,087	0,022	156,6
C7	10	10	60	1,064	0,016	159,9
C8	10	10	70	1,049	0,012	162,3
C9	10	10	80	1,039	0,010	164,2
C10	10	10	90	1,031	0,008	165,8
C11	10	10	100	1,026	0,006	167,0
C12	10	10	150	1,012	0,003	171,1

Table 3 – Cylindrical pillars structure, design characteristics

We notice that for the same parameters P, H and W, r and f are higher in the square pillars. We are interested in high values of r but in low values of f, for standard dropwise condensation in circular pillars, but for sweeping condensation there is not enough experience to know what will be better.

The SEM characterization showed the following results:

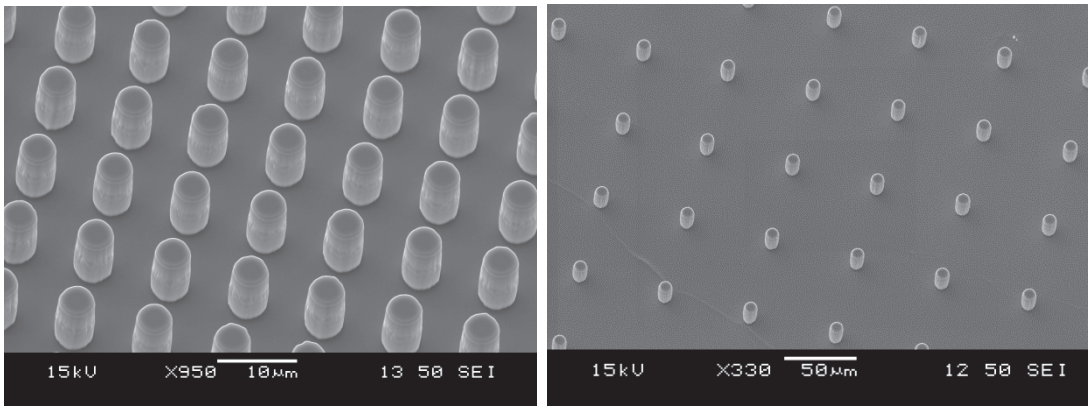

Figure 22 - Cylindrical micropillars SEM imaging a) P=10, b) P=60

As we can see the circular pillars don't show any important defect that can affect their wettability too much.

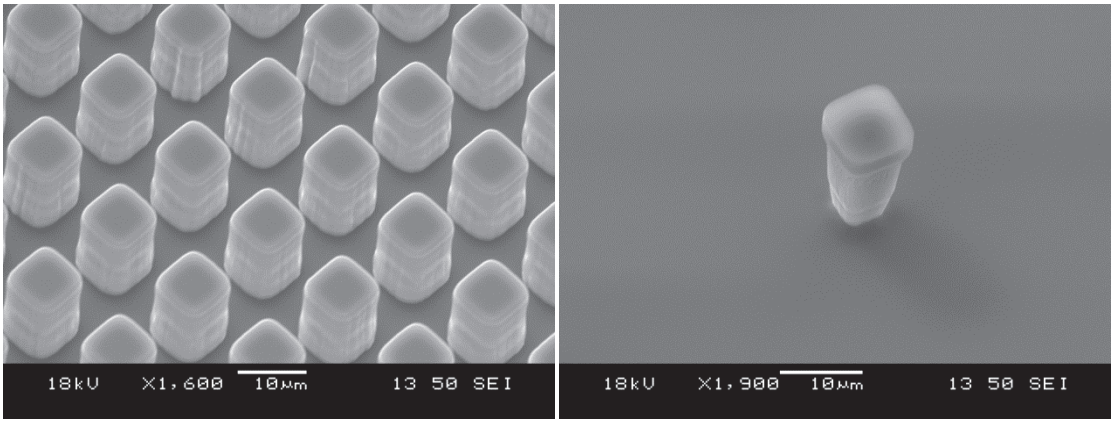

Figure 23 – Square shaped micropillars with W=10. They show different shape depending on the pitch a) P= 10 b) P=60

In the case of the square pillars we can see that for the 10µm width pillars, the quality of the corners depend a lot on the pitch of the pattern, when the pillars are near, the corners are better shaped and when the pitch is too large the shape gets worse, and with some scalloping.

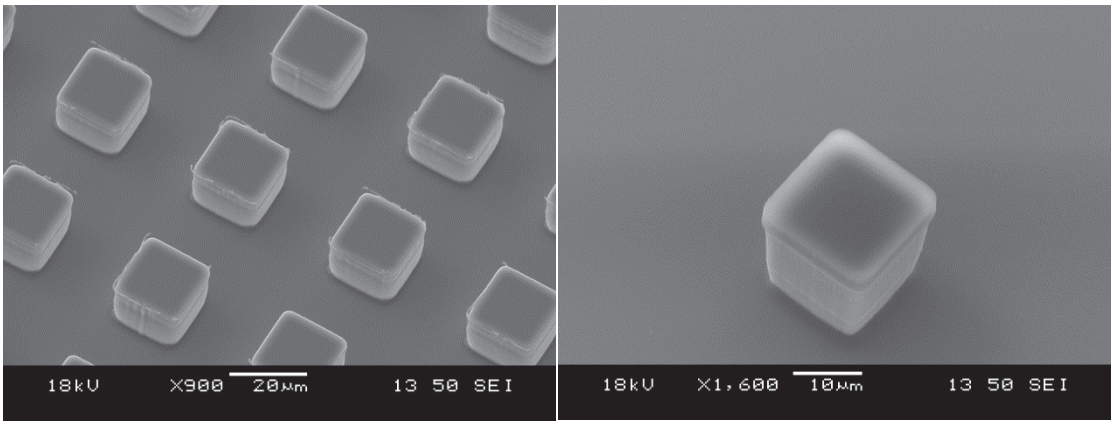

Figure 24 – Square shaped pillars with W=20. A) P=20, B) P=100

In the case of the wider square pillars we find that the corners are better shaped, and there is no big difference between the closer ones and the others with higher pitch.

We noticed that while the width and the pitch parameters are very good approximations of the desired values, the height values have a higher deviation. For the cylindrical pillars it was equal to H=8.9µm and for the square pillars it was H=11.3µm.

Now we are going to measure only the static contact angle to characterize the samples. To have robust results we clean all the samples before the measurent to eliminate all the organic contamination that influence our measurement. To avoid the effect of punctual defects we are going to take measures on three different spots of the sample and we will accept that the average value as the contact angle of the sample. The results of the contact angles are displayed in the following table:

Sample ID	CA (°) ±5°
C1	143,15
C2	125,62
C3	96,34
C4	82,31
C5	73,16
C6	65,32
C7	68,47
C8	61,86
C9	58,94
C10	56,27
C11	58,13
C12	55,04

Table 4 – Cylindrical pillars structures, contact angle measurements. The value measured is the arithmetic average of the three measurements realized in different spot of the same sample

The cylindrical pillars with SU8-5 top achieve high hydrophobicity in the cases with less pitch and the contact angle trend is decreasing as the pitch increases. We noticed that contact angles can vary around 4-5° on the same sample just measuring on different places. Also another errors can happen because sometimes the software doesn't recognizes the baseline when the droplet is very hydrophobic and the contact angle measurement has to be done again.

With the square pillars, the measures are quite different:

Sample ID	CA (°) ±5°
SQ1	15,08
SQ2	18,57
SQ3	19,32
SQ4	20,11
SQ5	18,61
SQ6	21,42
SQ7	23,1
SQ8	26,75

Sample ID	CA (°) ±5°
SQ9	13,35
SQ10	12,77
SQ11	19,34
SQ12	25,57
SQ13	27,34
SQ14	28,32
SQ15	24,74
SQ16	31,56

Table 5 – Square pillars structures, contact angle measurements. As the droplets occupy the whole sample only one measurement is made in every sample

As the theory says, a hydrophilic surface becomes more hydrophilic when roughness is placed in it, but these values are too low even for that. It was preferable a certain level of hydrophilicity, to have Wenzel state where the droplets are between the pillars. But with that very low contact angle maybe the droplets are too pinned to experiment any movement. Also, as the resulting droplet has an almost flat morphology, only one droplet spreads all over the sample, so the low contact angles measures are not because of punctual defects. It's possible that the intrinsic hydrophilicity has been enhanced by the presence of dust or organic contaminants in the surface, as the place where we measure the contact angles is not a cleanroom. However after a proper cleaning as we did with the cylindrical pillars the expected contact angle was higher than the actual was. The theoretical Wenzel contact angle applying the formula should be some times higher than the actual one.

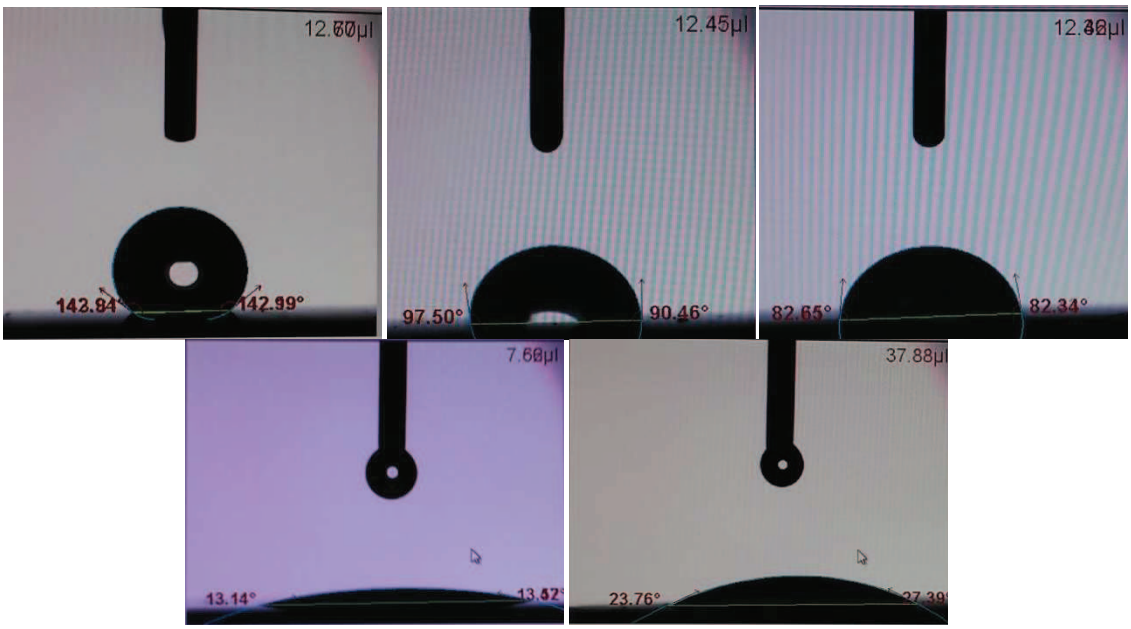

Figure 25 – Images taken during contact angle measurements showing the high contrast between the cylindrical pillars up (C1,C3, C4 respectively) and the square pillars down (SQ9 and SQ12 respectively). The images were taken from the computer screen with a camera.

5. Experimental setup for condensate droplets visualization

In this chapter we are going to describe the setup arranged to achieve the visualization of the condensation process.

5.1 Visualization techniques review

The most used techniques for visualization of droplet growth and coalescence includes the use of scanning electron microscopes allowing features smaller than a few micrometers. The equipment used can be an ESEM or an ETEM. Both microscopes can operate at different pressures but generally there are limited up to 2.7 kPa.

ESEM has been recently the most used technique for visualization (31). The advantages are that it allows gases in the sample chamber and control of the temperature of the sample and the pressure of the water vapor. With a proper adjustment of these parameters condensation can be reached under low pressures. Thus, dynamic droplet growth can be observed, contact angles can be measured, and individual droplet heat transfer rates can be calculated. However this technique has some drawbacks as the beam heating when imaging around 10μm and that normally the maximum speed is 10 fps. Despite there are some techniques to avoid the beam heating and some screen capture software that can achieve a rate about 55 fps, the limit on pressure of the ESEM makes the results obtained only guidelines that not necessarily will be followed in ambient or industrial conditions. As the ESEM that we have in the NTNU NanoLab doesn't have yet stage temperature control, we can't try to visualize condensation there.

The visualization setup that we propose is inspired in some utilized to view coalescence process and jumping of the droplets (44) however they used a speed of 3000fps. With the lighting devices that we have in the lab the highest speed that we can have is 50 or 60 fps which is very tiny compared to the speed that they used. With this low recording speed we are not going to be able to record the droplets jumping, but we could deduce the departure when the droplets disappear.

5.2 Experimental setup design

In this work we are going to visualize the condensation droplets using optic microscopy using a fast camera and different lenses. In the first place we imaged the cylindrical

pillars from a side of the sample having a LED light with controllable intensity up to 1.6 A. Later when imaging the square pillars this technique didn't work due to the corners of the pillars, which makes it difficult for the light to reach the camera. Then we used a top view by using a mirror and to increase light we used an optic fiber.

The camera used is a FastCam Photron (ThorLabs). The speed selected was 50-60 fps according to the light that we had. CF-4 tube and S58 tubes were utilized for the upside view while another one with zoom option was used in the side view. The camera is attached to a rail, which allows changing the distance of the camera with some precision maintaining the tilting and the visualization direction.

Figure 26 – Photron Fastcam (Thorlabs) setup with the second disposition lenses.

To achieve condensation we need a cooler element. We have used a Thermo Electric Cooler (Peltier element) that can reduce the temperature of one side and increase the temperature of the other side. If we want it to work well we need to cool down the hot side of the Peltier element. The sample is over a stage that allows us tilting, rotating and moving it small distances easily.

In the first design of our setup for the experiments we used a computer fan to cool down the backside of the Peltier element and no vapor were over the sample, it is performed at ambient conditions. With this setup we can test the lenses of the camera and choose the one that offers the best imaging.

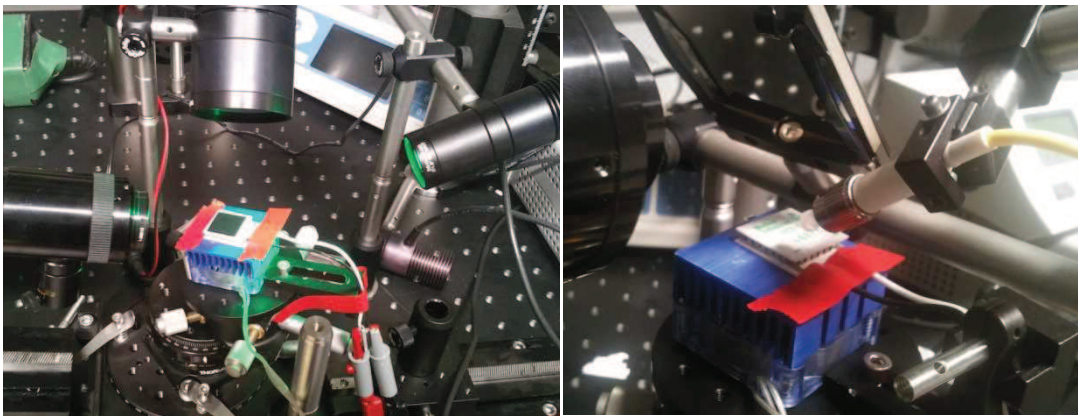

Figure 27 – Samples stage and setup. Left: First setup with the green LED and the camera recording the side view. Right: Second setup with the mirror at 45° approximately to record the upside view and the optic fiber for the lighting.

We used a variable DC source to feed the Peltier element and the computer fan. The voltage selected was 2.09 V for the Peltier and 11.23 V for the computer fan. This voltage remained like that and current only flow when the output power button was activated. These parameters give a temperature in the cold side of the Peltier element around 14°C.

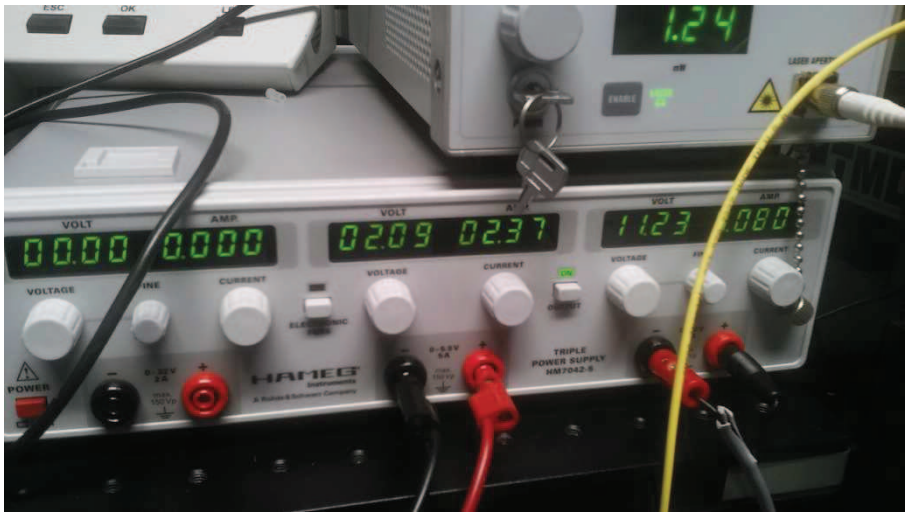

Figure 28 – DC voltage source with the Thermo Electric Cooler connected to the middle source and the computer fan connected to the right source.

To do the experiment at controlled conditions of water vapor saturations and reduction of the presence of non condensable gases (NCG) that affects negatively to the dropwise condensation process another setup has been designed.

This setup consist on a chamber of Plexiglas 10 mm thick with four tubes for steam flowing and a thin glass circle of 50 mm diameter for the lens of the camera. This chamber tightly fits in a thermal insulator material base sealed with blue silicon and

with a small square space where the cooling system is. The cooling system is composed by a Peltier element, a cooper chip and a cooper cooler which has cold glycol flowing through it. The glycol is cooled with a chiller.

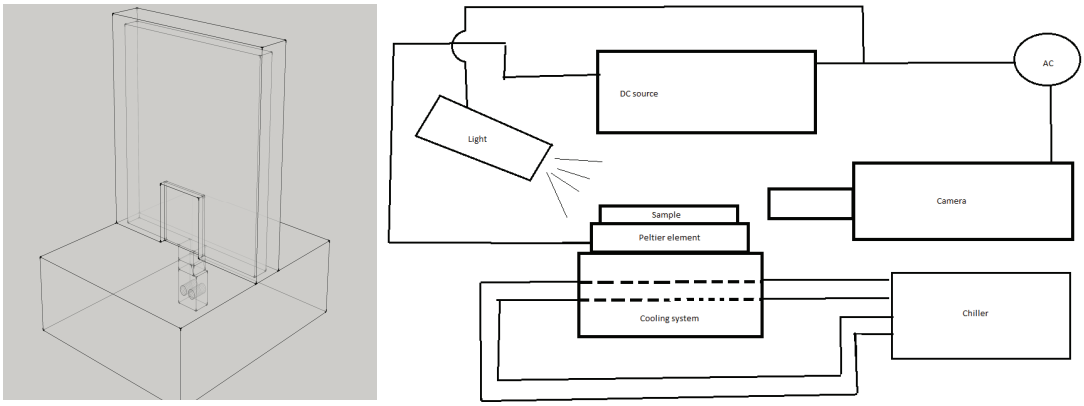

Figure 29 – Condensation chamber design and instrumentation diagram design

This setup has been fabricated but with too much delay, making it impossible to use it in this work, however the chamber is finally done with some variations for easy fabrication and can be used in further projects.

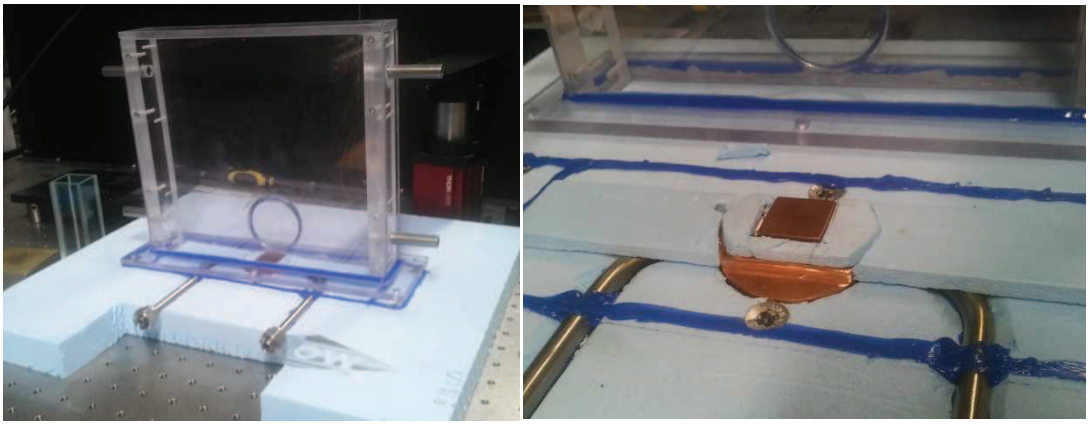

Figure 30 – Condensation chamber setup and stage inside the chamber.

Controlling the cooling temperature and with some thermocouples in the chamber, we should also be able to measure heat flux. This measure will not be very accurate, but when we want to compare the heat flux through different surfaces, that will provide a reasonable comparison. The glass for visualizing the droplets should be heated up with warm air to avoid condensation on it. The amount of air in the steam flow can be reduced running the steam generator for half an hour for example.

5.3 Results

We started the experiments with the cylindrical pillars. We started the setup procedure and when we started to see nucleation, we started the recording function of the camera. The recording time of the camera is up to 100 seconds approximately, depending of the resolution of the image. We used low resolutions to record only what it was in the focus range. As in the first lenses composition we had a very narrow depth of field, we can use very low resolution enlarging the recording time. The video was afterwards compressed using windows movie maker.

5.3.1 Cylindrical pillars

The image obtained by using the first disposition wasn't very good for visualizing pillars with low pitch because the light gets trapped between the pillars and as they are so close we only can see the top of the pillars. To complement the image obtained here an upside view with the second disposition was made. In the second disposition we also had some disadvantages, like that we couldn't use zoom so the image that we get doesn't have good level of detail. But studying the two images together we can realize what is happening between the pillars and at what height. We can't have the two images for the same time or area, but in a general trend we can relate the two images to obtain conclusions about the process.

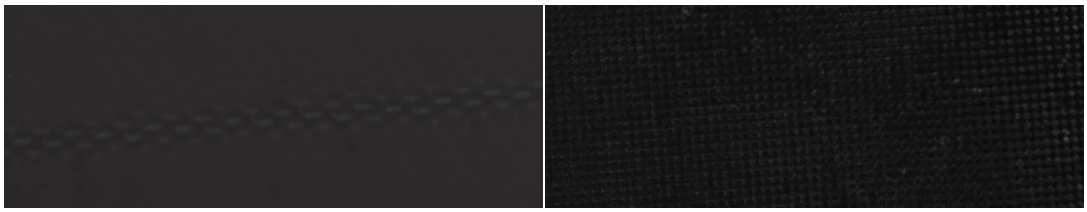

Figure 31 – Side view and upside view of cylindrical micropillars with 5µm pitch

For pitch values higher than 20µm we achieved a good image of the pillars and it's not that necessary to have an upside view to know what is happening between the pillars. We must notice that for high pitch values, we start to see the shadow of the pillar and it isn't a strange shape of the pillars.

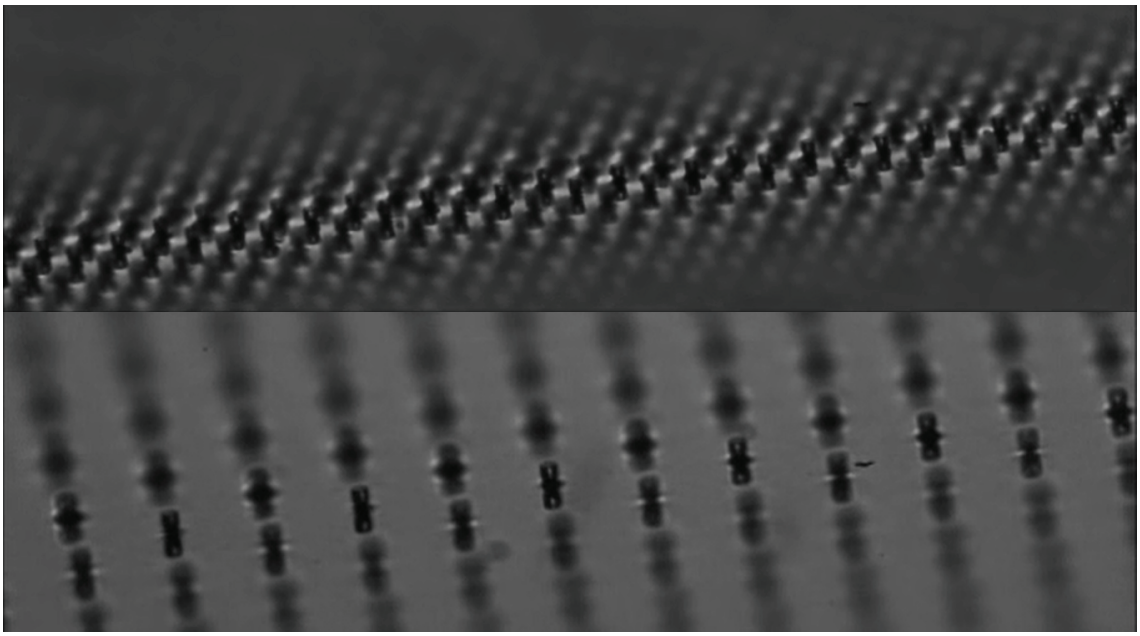

Figure 32 – Side view of pillars with pitch equal to 20 and 60µm

The image of the pillars is quite good for these spaced pillars, but when water starts to condense, everything changes. The light is reflected, refracted or absorbed by the water and the image becomes very dark.

We start with the pillars with the highest spacing because the image has the best quality.

For example analyzing the videos obtained with the P=100 sample, we can find an early stage of nucleation clearly taking place in the space between the pillars. At first small droplets appear in all the surface and then they start to coalesce growing bigger. Also we can observe that if the droplets touch a pillar they tend to grow around it, and when they coalesce, the resulting droplet is also around the pillar. As the water is condensing it seems that the depth of field goes narrow and we only can see in a narrow line.

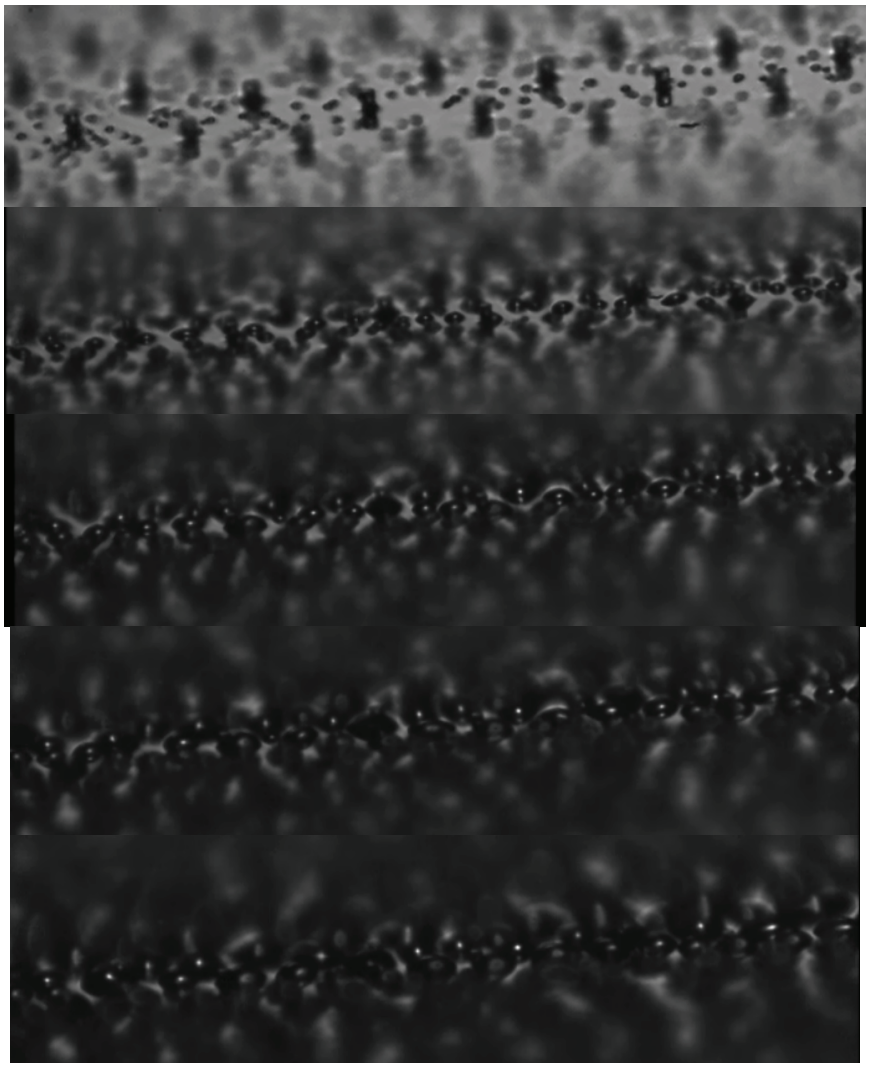

Figure 33 – Side view of condensation process in pillars with P=100µm

The recording time is not long enough to see the flooding but it eventually occurs. As the individual droplets grow bigger and bigger they start to occupy all the space and a continuous film appears covering the pillars. All the droplets seem to be in a pinned Wenzel state, so jumping is not possible in this structure.

The same process occurs with the samples with pitch equal to 150, 90, 80 and 70. When we study the samples with lower pillar interspacing the image is darker and more difficult to interpret.

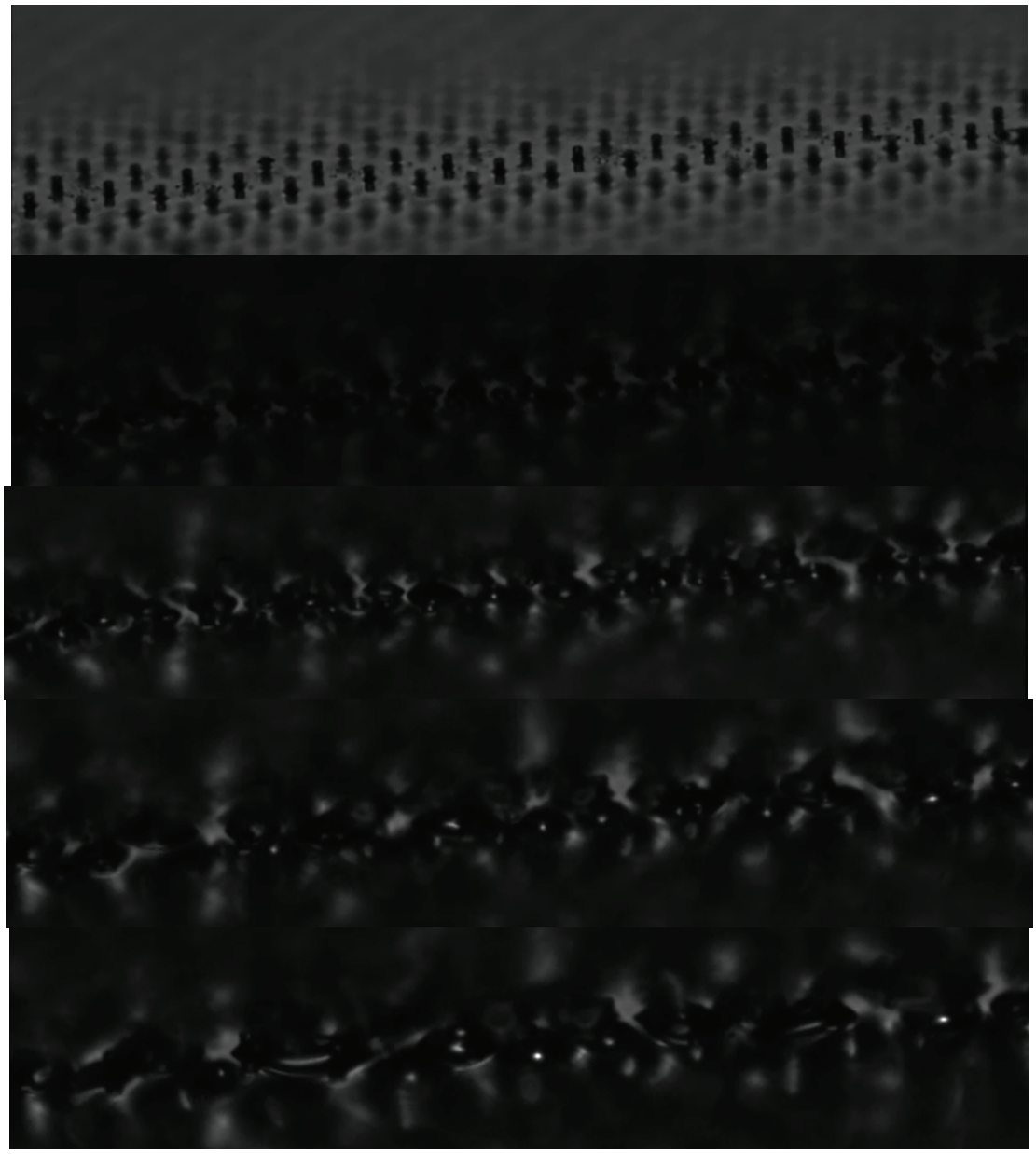

Figure 34 – Side view of condensation process in pillars with P=60µm

With pitch equal to 60 we still can distinguish what's going on with the droplets, but for lower pitches, the image gets more confusing and we require an upside view to analyze it.

The upside view is helpful to know what is going on in the between of the pillars, but has a lack of information because it covers wide areas without the possibility of zoom in. On the one hand, we won't be able to distinguish the droplets shapes as easily as before, but on the other hand we will have a better view of the coalescing events over a wider area than before.

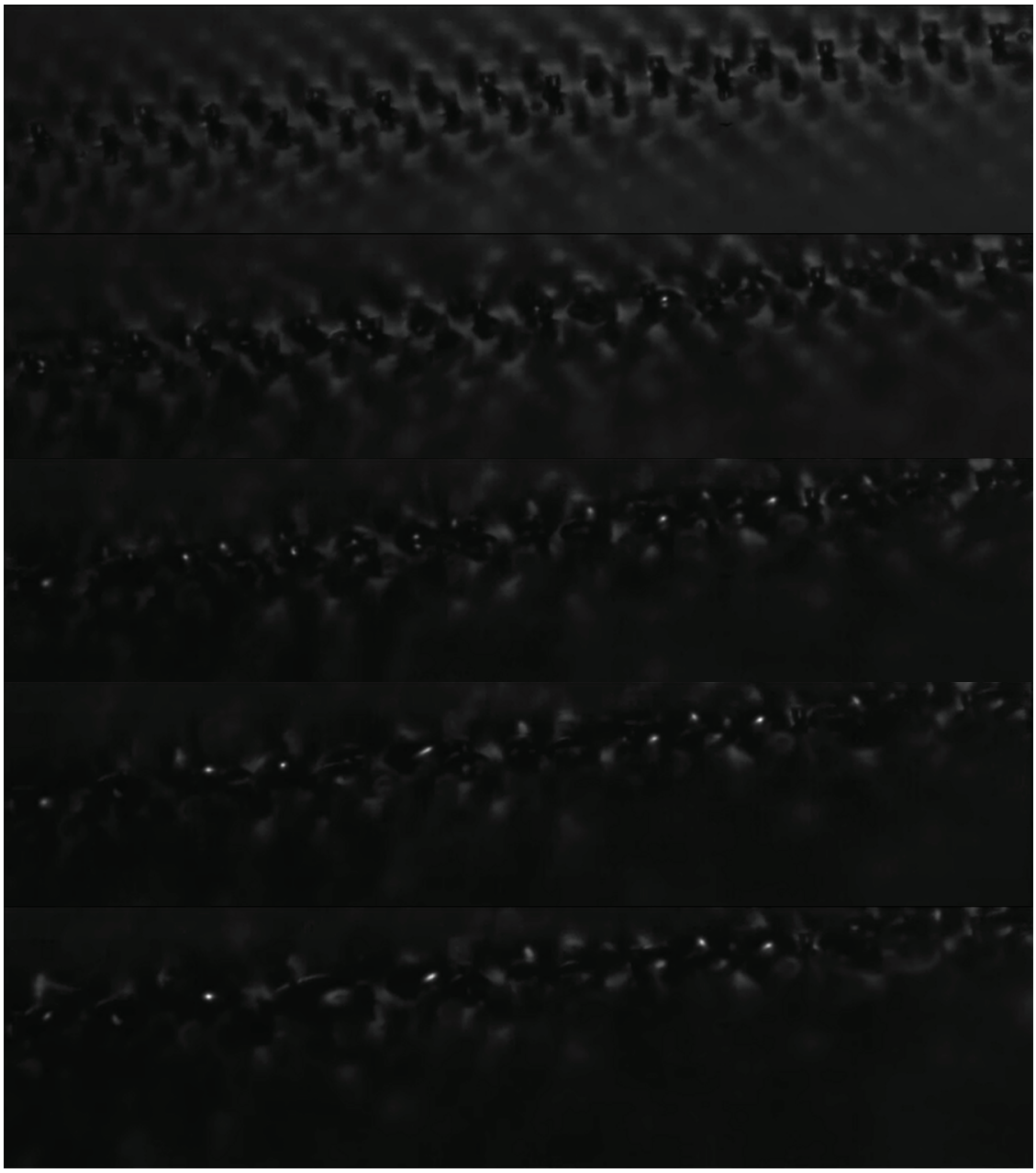

Figure 35 – Side view of condensation process in pillars with P=40µm

As we can see in the Figure, the droplets seem to nucleate directly around the pillars for this low pitches but as we can see in the upside view, the nucleation process doesn't take place in the pillars, it occurs in the space between them. Once that the nucleation occurs, in the upside view we can't distinguish very well where the pillars exactly are as the droplets have the same shape.

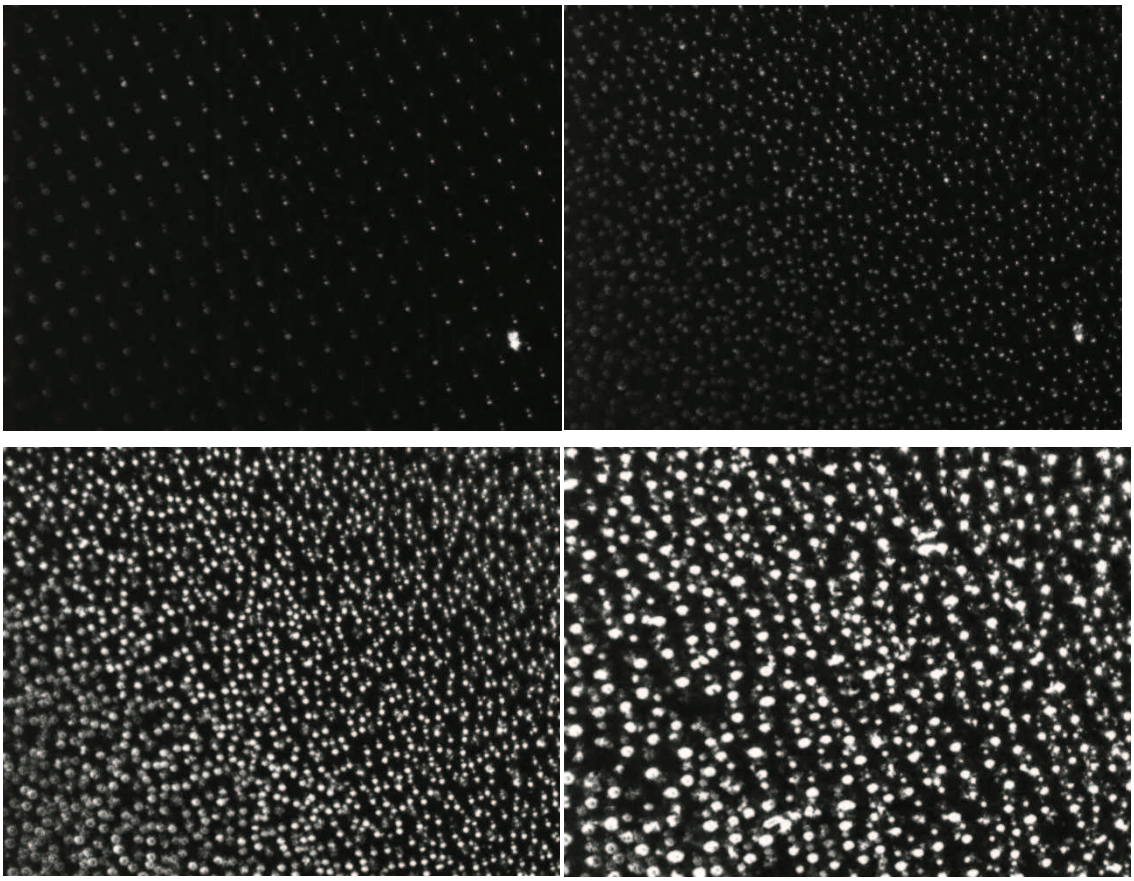

Figure 36 – Upside view of condensation process with P= 40µm

Between the two last images of the figure a lot of coalescences were observed. We find that the coalescences were randomly distributed over the space and there was not anything related between them, for example, one of them didn't caused more coalescence as in the chain coalescence typical of the sweeping droplet removal mechanism. If we go for lower pitches as 30 or 20µm exactly the same is happening with only one difference: when the droplets grow bigger, they become pinned with four pillars, filling all the space between them.

With the samples with 5 of pitch, we started to see small Cassie droplets over the top of the pillars. In fact, with the side view we only can see these Cassie droplets until the film formed between the pillars reaches their top. With the upside view we can see that there is droplets emerging in the space between the pillars and they coalesce until a film is formed and grows to the top of the pillars.

Figure 37 – Side view of condensation process in pillars with P=5µm

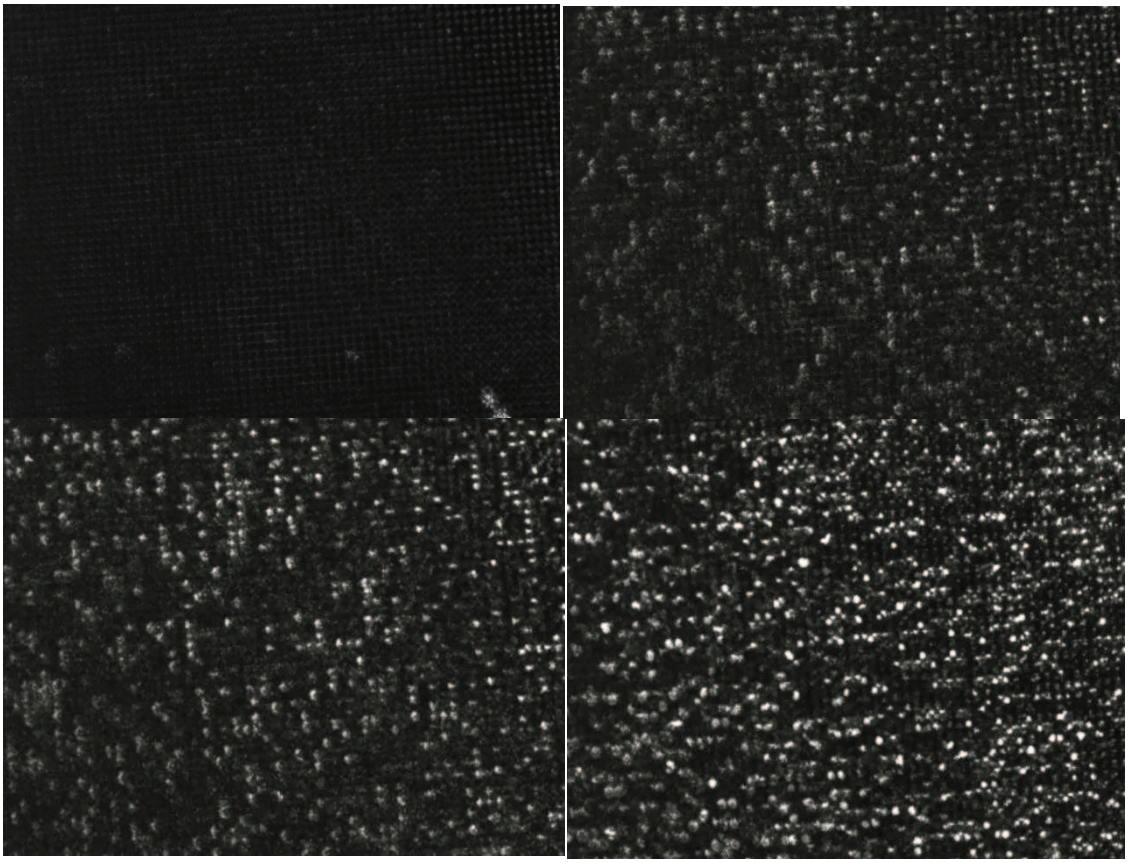

Figure 38 – Upside view of condensation process in pillars with P=5µm

5.3.2 Square pillars

Now we go with the square pillars. When trying to visualize the small square pillars with 10 of pitch, we noticed that the corners have a very important role in the visualization. Even in the highest pitches we couldn't see almost anything with the side view, so square pillars are only visualized with the upside view.

Starting with the highest pitch values for the low width pillars, we find that the nucleation, grown and coalescing processes are quite faster than in the cylindrical pillars. It is so fast that is difficult to record the time when the nucleation starts. We could suppose that before than doing the experiment because of the high hydrophilicity of the samples.

We find that in this case, the top of the pillars play an active role in the nucleation and the growing and coalescing process. Some droplets nucleate on the top of the pillars and they coalesce between them forming a big droplet on them. This droplet start coalescing with the neighboring droplets that aren't in any pillar, forming a bigger droplet attached to the pillar. Thus, the area around the pillars becomes dry and new nucleation appears. This is repeated until the droplets attached to the pillars leave no space between them for new nucleation. Once that it happens, the droplets coalesce linking the pillars with a big droplet that at the end tends to become a liquid film.

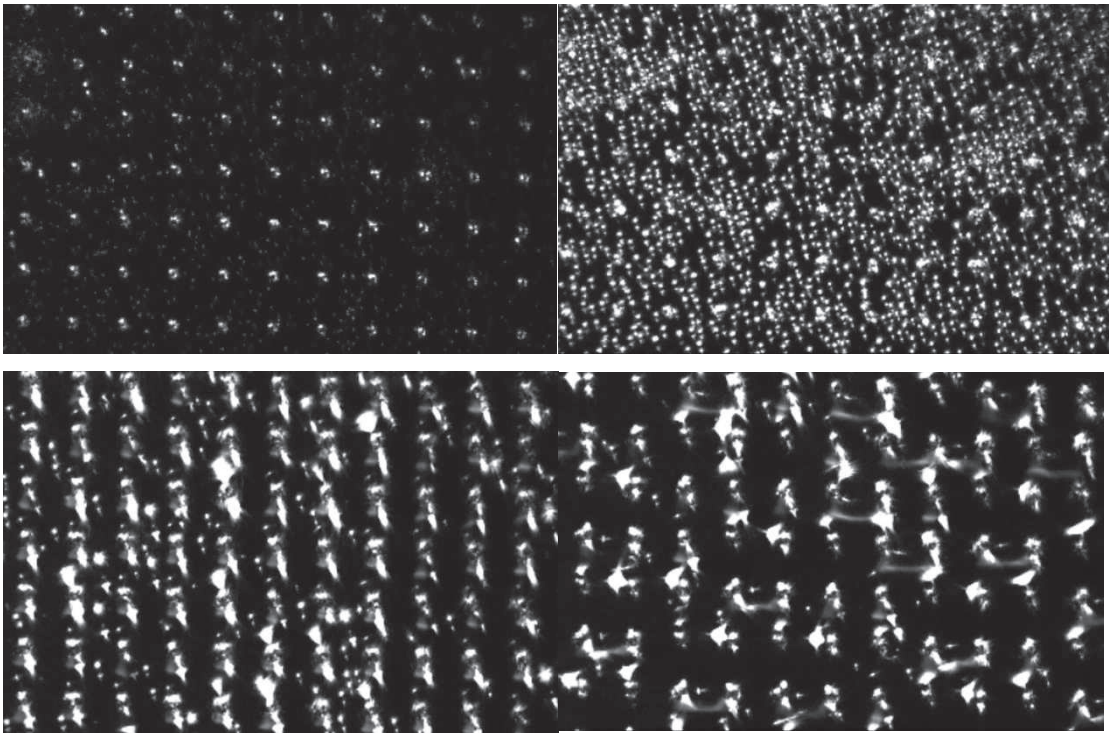

Figure 39 – Upside view of condensation process in pillars with P= 60µm W=10µm

This setup for imaging has certain lack of information because we don't know what kind of droplets are formed. However we will assume, judging by the contact angles showed for bigger droplets that the condensation droplets will be also in Wenzel state with low contact angles.

This process occurs in samples with pitch values equal to 70, 60, 50, 40, and even 30. With a pitch equal to 20 and lower is more difficult to distinguish if the same process is taking place, and even assuming that is the same process, as the pillars are so close, the droplets will form a film linking the pillars much before.

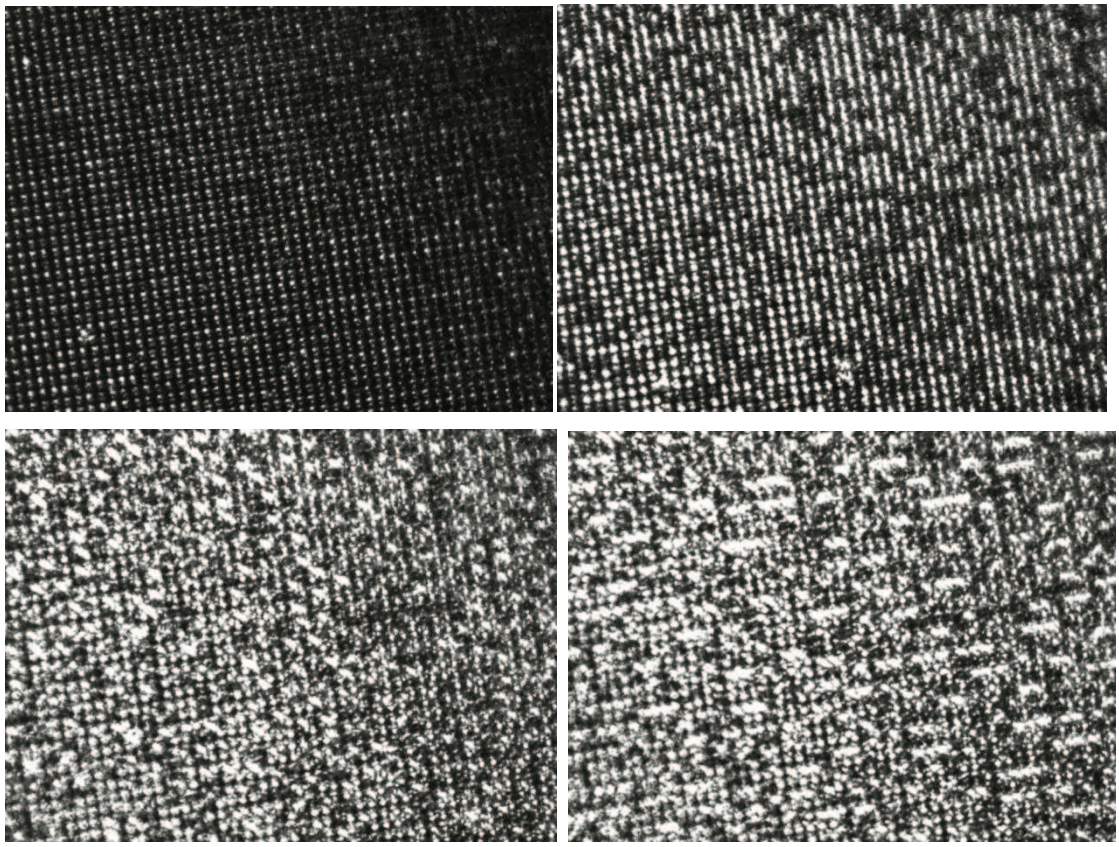

Figure 40 – Upside view of condensation process in pillars with P=10µm, W=10µm

In the third image we can barely see that droplets are formed linking four adjacent pillars, but this step last a few instants because the droplet coalesce with some others forming a liquid film soon.

Now we are going to experiment with the big square pillars, starting with the highest pitch values. As we could expect from our experience with the small square pillars, we find that for these high spaced pillars the process is more or less the same. However as

the dimensions here are bigger, the droplets between the pillars grow bigger and acquire more importance in the process.

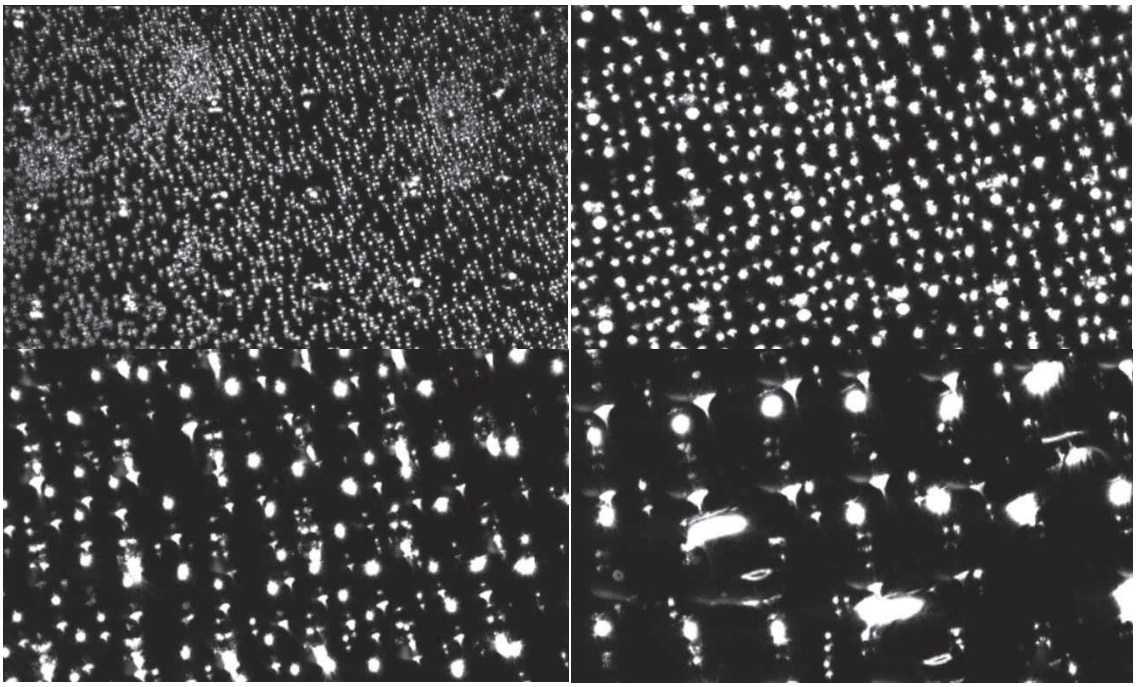

Figure 41 – Upside view of condensation process in pillars with P= 100µm W=20µm

We find that this process is followed by all the samples. In this case we have a good image of the samples with smaller pitch. And with the difference that the flooding occurs before than in the others with more pitch, the process has the same steps.

Despite the droplet growing and coalescence process is different in the square pillars than the described before for the cylindrical pillars, we didn't achieved the visualization of the droplet removal mechanism. As described avobe, with this light and camera parameters, it was not expected to record the droplets jumping, but the chain coalescence mechanism should be possible to record, or at least the space that the droplets departure left.

5.3.3 Discussion

Comparing square and cylindrical pillars we have some differences in the droplets behavior between them. One of the fundamental ones is that in the square pillars, nucleation is started in the top while in the cylindrical pillars it is not, as it is covered with SU8. This seems to be very important in the posterior growing and coalescing of the droplets, because in the square pillars, bigger droplets are formed pinned to the pillar while in the cylindrical pillars they are not. It is important to notice that in the

cylindrical pillars the droplets in the space between the pillars are bigger, so they have more influence in the condensation regime as when they start to link several pillars, then flooding is soon appearing.

Analyzing the videos it can be seen that when the bigger droplets start the flooding of the surfaces, they link the four adjacent pillars, and until there are many of them in this disposition there is not linking with more than four pillars. That happened in every structure with the exception of the smallest and the biggest ones. In the first case because the flooding starts too soon and the film formed links all the pillars and grow until it reaches the tops. And in the second case because the distance between the pillars is so big that when a droplet is linking four pillars it is necessarily a film.

6 Conclusion

6.1 Summary and conclusions

In this document, we have studied the mechanism of dropwise condensation and the methods to achieve it modifying the surface. We have found that this mechanism is very complex and it's not easy to obtain under laboratory or industrial conditions.

The review of the literature and the previous experiments showed the different ways to approach DWC, but all of them are still in lines of developments without a precise answer on how to sustain DWC. Continuing with one of the latest innovations on this topic we tried to achieve sweeping condensation on a one-tier-roughness microstructured surface, making a comparison between the important elements in this surface (having corners or don't having it). For this purpose, several structures with different roughness characteristics were designed covering a range of r between 1 and 3 and f between 0.5 and 0.05. Having constant H/W for the cylindrical pillars and two values of H/W 1 and 0.5; we have focused on the study of the pitch and how it affects to the condensation process.

Then, the process of photolithography was studied and performed in order to fabricate the desired microstructures. Finally the design of the samples was achieved without important defects in the structures. The samples were characterized using a Scanning Electron Microscope and their wetting properties were measured via the measurement of contact angles. The result of these measurements was surprising and unexpected in the case of the square pillars, where high degree of hydrophilicity was discovered.

But to know how the condensation process is going, a visualization setup should be done. After reviewing the most common methods in the literature, some experimental setups were designed and built. Due to the lack of time, only one of the setups thought was launched. Some pre-experiments have been made in order to calibrate all the parameters in the camera, stage and cooling devices. Once that every device was ready for the experiments the samples were tested under laboratory conditions.

From the analysis of the data obtained we found the limitations on the experimental setup for low pitch values. We also could determine that the samples that we made didn't showed DWC or sweeping condensation as we expected. The process occurring

on the different samples was identified and discussed, highlighting the differences between the square pillars and the cylindrical pillars.

6.2 Recommendations for further work

In this thesis two main tasks were performed; one was the designing and fabrication of microstructured surfaces and the other was the designing and fabrication of an experimental setup to achieve the visualization of the condensation process.

Regarding the first part of the thesis and judging by the results obtained in the second part, we have found that a one-tier-roughness is not useful to lead to DWC mode as no self-induced droplet removal was observed in the experiments. This is why more researching has to be done in the topic of coatings to obtain a hierarchical structure. A laboratory method should be made to achieve the desired characteristics on the coating of the surface. Once that a hierarchical structure is obtained it can be tested and compared in the different setups that have been designed in this thesis.

Regarding the second part of this thesis, there's a lot of improvement to be done, starting with the testing of the condensation chamber setup that we designed and made. Limitations on the camera have been found and better lenses or proper tools to visualize condensation in the ESEM can be studied to improve the imaging process. Also, heat transfer measurements can be rudimentarily done in the condensation chamber, but further study of the characteristics of the setup or the measurement process will lead to better results.

Appendix A: Recipes

A.1 Recipe for micro pillar fabrication in 4” wafer

Made by Il-Woong, Eivind and Øyvind.

1) Cleaning of Si wafer
    - ❖ Acetone bath in beaker, gently stirring in circles
    - ❖ Lift up the wafer while showering with Ethanol
    - ❖ Continue showering with Isopropanol
    - ❖ Continue showering with DI water
    - ❖ Dry with N_2
2) Dehydratation
    - ❖ 200°C for 5 min
3) Plasma cleaner
    - ❖ 3min at 50%O_2 and 50% power
4) Photoresist spinning coating
    - ❖ SU8-5
    - ❖ Parameters: 3000rpm – 30sec – 300rpm/sec
    - ❖ This gives a photoresist thickness of 4-5µm
5) Pre Exposure Soft Baking
    - ❖ Use your own clean 4” carrier wafer on the plate
    - ❖ Temperature: 65 degrees for 1 min
    - ❖ Increase temperature to 95 degrees with wafer on the plate
    - ❖ Temperature: 95 degrees for 3 min
    - ❖ Cool down for 3 min on plate
6) Control backside, clean with acetone if necessary
7) UV exposure
    - ❖ Type: MA6
    - ❖ Energy: 200mJ
    - ❖ Method: Hard
    - ❖ Distance: 100 (only for alignment)
8) Post Exposure Soft Baking
    - ❖ Use you own 4” carrier wafer on the plate
    - ❖ Temperature: 65 degrees for 1 min

- Increase temperature to 95 degrees with wafer on plate
- Temperature: 95 degrees for 2 min
- Cool down for 3 min on plate

9) Measure of resist thickness on reflectometer
10) Development
    - Type: Dev-600
    - Steps (repeat 3 times):
        i. Development bath for 1.5 min
        ii. Water bath
        iii. N2 stream
11) Dehydratation
    - 200°C for 5 min
12) Etching
    - Type: ICP-RIE Cryo
    - Time: depending on the recipe
    - Gas: SF_6 and O_2
    - Conditioning of main chamber: sun same recipe with a dummy wafer
    - Run the chamber clean recipe before the conditioning if Cl_2, BCl_3 or HBr were run before
13) Image and measure of micropillars' height with JEOL SEM
14) Eliminate residues of photoresist on top of micropillars in the ICP-RIE Cryo using O_2 cleaning 30 min recipe

A.2 ICP-RIE Cryo Recipe

A.2.1 Recipe for cylindrical pillars

Steps 4, 5, 6 and 7 are in a loop that is repeated 4 times to get 10µm height

1) HE Leak Check (STD) – 10 sec
2) Pump (STD) – 3 min
3) N_2 Purge (STD) – 2 min
    - P=40 mTorr
    - T= -120°C
    - N_2= 100sccm

4) Pump to $1e^{-6}$ (STD)
5) Strike – 8 sec
    - P= 10 mTorr
    - T= -120°C
    - RF=40 W
    - ICP= 600 W
    - O_2= 10 sccm
    - SF_6= 60 sccm
6) Etch – 2.5 min
    - P= 10 mTorr
    - T= -120°C
    - RF= 6 W
    - ICP= 600 W
    - O_2= 10 sccm
    - SF_6= 60 sccm
7) N_2 Purge (STD) – 3 min
    - P=40 mTorr
    - T= -120°C
    - N_2= 60sccm
8) Loop (STD) – 3 times
    - N_2 Purge
    - Pump
9) Pump to $1e^{-6}$ (STD)

A.2.2 Recipe for square pillars

Steps 4, 5, 6 and 7 are in a loop that is repeated 4 times to get 10µm height

1) HE Leak Check (STD) – 10 sec
2) Pump (STD) – 3 min
3) N_2 Purge (STD) – 2 min
    - P=40 mTorr
    - T= -120°C
    - N_2= 100sccm
4) Pump to $1e^{-6}$ (STD)
5) Strike – 8 sec

- P= 10 mTorr
- T= -120°C
- RF=40 W
- ICP= 600 W
- O_2= 8.5 sccm
- SF_6= 60 sccm

6) Etch – 2.5 min
   - P= 10 mTorr
   - T= -120°C
   - RF= 6 W
   - ICP= 600 W
   - O_2= 8.5 sccm
   - SF_6= 60 sccm
7) N_2 Purge (STD) – 3 min
   - P=40 mTorr
   - T= -120°C
   - N_2= 60sccm
8) Loop (STD) – 3 times
   - N_2 Purge
   - Pump
9) Pump to $1e^{-6}$ (STD)

A.2.3 ICP-RIE Ctyo O2 Cleaning Recipe

1) HE Leak Check (STD) – 10 sec
2) N2 Purge (STD) – 2 min
   - P = 40 mTorr
   - T = 20 °C
   - N2 = 100sccm
3) Pump to 1e-6 (STD)
4) O2 Clean – 30 minutes
   - P = 10 mTorr
   - T = 20 °C
   - RF = 200 W

- ICP = 1500W
- O2 = 40 sccm

5) Loop (STD) - 3 times
   - N2 Purge
   - Pump - 3 minutes
6) Pump to 1e-6 (STD)

A.3 Breaking Parameters

- General
  - Wafer diameter: 102 mm
  - Wafer thickness: 550µm
- Scribe parameters
  - Method: Continuous
  - Impulse bar height: 0µm
  - Scribe Extension: 90µm
  - Scribe Force: 1900cnts
  - Scribe Angle: 36 deg.
  - Scribe Speed: 2.4 mm/s
  - Approach Speed: 3.8 mm/s
- Break Parameters
  - Method: Anvil
  - Pressure: 75 kPa
  - Anvil Height: 0.736 mm
  - Anvil Gap: 0.686 mm
  - Dwell Time: 0.1 sec
  - Cycle Time: 0.2 sec

Bibliography

1. *Three-Dimensional Hierarchical structures for Fog Harvesting.* **Andrews, H.G.** 2011, Langmuir.

2. *High efficiency electric power generation: The environmental role.* **Beer, J.M.** s.l. : Progress in Energy and Combustion Science, 2007.

3. *Design of an Integrated Loop Heat Pipe Air-Cooled Heat Exchanger for High Performance Electronics.* **Peters, T.B., et al.** 2012, Transactions on Components packaging and Manufacturing Technology, pp. 1637-1648.

4. *Advances in seawater desalination technologies.* **Khawaji, A.D., I.K.Kubkhanah and J.M.Wie.** 2008, Desalination, pp. 47-49.

5. *A review on buildings energy consumption information.* **Perez-Lombard, L., J. Ortiz, and C. Pout.** 2008, Energy and Buildings, pp. 394-398.

6. *Urbanisation and its impact on building energy consumption and efficiency in China.* **Li, B.Z. and R.M. Yao.** 2009, Renewable Energy, pp. 1994-1998.

7. *Surface Engineering for Phase Change Heat Transfer: A Review.* **Attinger, D. et al.** 2014, MRS Energy and Sustainability, a Review Journal, pp. 15-21.

8. *Convective Heat Transfer.* **Bejan, A.** 2003, Wiley.

9. *Self-propelled sweeping removal of dropwise condensate.* **Boreyko, J.B., et al.** 2015, Applied Physics Letters.

10. *Wetting and roughness .* **Quéré, D.** 2013, Annual Review of Materials Research, pp. 71-99.

11. *Contact Angle, Wettability and Adhesion.* **Zisman, W.A.** 1964, Advances in Chemistry, American Chemical Society, pp. 1-6.

12. **Scientific, Blloln.** OneAttension Theta user manual Rev2.31.

13. *Resistance of Solid Surfaces to Wetting by Water.* **Wenzel, R.N.** 1936, Ind. Eng. Chem., pp. 688-994.

14. *Wettability of Porous Surfaces.* **Cassie, A.B.D. and S.Baxter.** 1944, Trans. Faraday Soc., pp. 546-551.

15. *Dropwise condensation on superhydrophobic surfaces with two tier roughness.* **Chen, C-H. et al.** 2007, Applied Physics Letters.

16. *Versuche über die Kondensation von wasserdampf In Film- und Tropfenform.* **Schmidt, E., W. Schurlg and W. Sellschopp.** 2, 1930, Tech. Mech. Thermodyn, Vol. 1, pp. 53-63.

17. *Effect of droplet Morphology on Growth Dynamics during Condensation on Superhydrophobic Nanostructured Surfaces.* **Miljkovic, N., R.Enright, and E.N.Wang.** 2012, Acs Nano, pp. 1776-1785.

18. *Self-Propelled Dropwise Condensate on Superhydrophobic Surfaces.* **Boreyko, J.B. and Chuan-Hua Chen.** 2009, Phys. Rev. Lett.

19. *Dropwise condensation theory and experiment: a review.* **Rose, J.W.** 2002, Proc Instn Mech Engrs, Vol. 216.

20. *Design and Fabrication of a Hybrid Superhydrophobic-Hydrophilic Surface that exibits Stable Dropwise Condensation.* **Mondal, B., et al.** 2015, American Chemical Society.

21. *Study of an Idealized Rough Surface.* **Dettre, R.H. and Jhonshon, R.E.** 1964, American Chemistry Society, pp. 112-135.

22. *Mimicking natural superhydrophobic surfaces and grasping the wetting process:A review on recent progress in preparing superhydrophobic surfaces.* **Y.Y. Yan, N. Gao , W. Barthlott.** 2011, ELSEVIER.

23. *Raster-Elektronenmikroskopie der Epidermis-Oberfachen von Spermathopyten.* **Barthlott, W.** 1977, Mainz, Wiesbaden: Akademie der Wiss. u.d. Literatur.

24. *Superhydrophobic surfaces: From natural to biomimetic to functional.* **Guo, Z., W. Liu and B.-L. Su.** 2011, Journal of Colloid and Interface Science, Vol. 353, pp. 335-355.

25. *Dicersitty of structure, morphology and wetting of plant surfaces.* **Koch, B.Bhushan and W. Barthiott.** 10, 2008, Soft Matter, Vol. 4, pp. 1943-1963.

26. *Recent advances in designing superhydrophobic surfaces.* **Celia, E. et al.** 2013, Journal of Colloid and Interface Science, pp. 1-18.

27. *Micro-, nano- and hierarchical structures for superhydrophobicity, self-cleaning and low adhesion.* **Bushan, B., Y. C. Jung and K. Koch.** 2009, Phil. Trans. R. Soc. A, Vol. 367, pp. 1631-1672.

28. *Superhydrophobic Surfaces.* **Minglin, M. and R.M. Hill.** 2006, Current Opinion in Colloid & Interface Science, Vol. 11, pp. 193-202.

29. *Wetting, adhesion and friction of superhydrophobic and hydrophilic leaves and fabricated micro/nanopatterned surfaces.* **Bhushan, B. and Jung, and Y.C.** s.l. : J. Phys. Condens. Matter, 2008, Vol. 20.

30. *Hierarchical roughness makes superhydrophobic states stable.* **Nosonovsky, M. and B. Bhushan.** 3, 2007, ELSVIER, Vol. 84, pp. 382-386.

31. *Dropwise Condensation on Micro- and Nanostructured Surfaces.* **Enright, Ryan et al.** 3, 2014, Nanoscale and Microscale Termophysical Engineering, Vol. 18, pp. 223-250.

32. *Mimicking the Stenocara Beetle - Dewetting of Drops from a Patterned Superhydrophobic Surface.* **Dorrer, C. and J. Rühe.** 2008, Langmuir, pp. 6154-6158.

33. *Mimicking a Stenocara Beetle's Back for Microcondensation Using Plasmachemical Patterned Superhydrophobic-Superhydrophilic Surfaces.* **Garrod, R.P. et al.** 2007, Langmuir, Vol. 23, pp. 689-693.

34. *Wetting behavior on hybrid surfaces with hydrophobic and hydrophilic properties.* **Yao, Chung-Wei et al.** 2014, Applied Surface Science, Vol. 290, pp. 59-65.

35. *Controlling nucleation and growth of water using hybrid hydrophobic-hydrophilic surfaces.* **Varanasi, K.K. and Tao Deng.** 2010, IEE, pp. 1-5.

36. *Recurrent Filmwise and Dropwise Condensation on a Beetle Mimetic Surface.* **Hou, Y. et al.** 1, 2015, ACS nano, Vol. 9, pp. 71-81.

37. *Using amphiphilic Nanostructures to Enable Long-Range Ensemble Coalescence and Surface ejuvenation in Dropwise Condensation.* **Anderson, D.M. et al.** 4, 2012, ACS Nano, Vol. 6, pp. 3262-3268.

38. *Condensation Enhancement with Micro and Nanostructured Amphiphilic Surfaces.* **Kottke, P.A., D.M. Anderson and A.G. Fedorov.** 2012, PowerMEMS, pp. 331-335.

39. **Anderson, D.M.** *THEORETICAL AND EXPERIMENTAL INVESTIGATION OF CONDENSATION ON AMPHIPHILIC NANOSTRUCTURED SURFACES.* Georgia : Georgia Institute of Technology, 2013.

40. *Über das Abspringen von Tropfen bei der Kondensation von Quecksilber.* **Kollera, M. and K. Grigull.** 1, 1969, Heat and Mass Transfer, Vol. 2, pp. 31-35.

41. **Preston, Daniel J.** Research: Daniel J. Preston . *Daniel J. Preston website.* [Online] 2016. [Cited: July 12, 2016.] http://www.mit.edu/~dpreston/research.htm#jumping.

42. **Miljkovic, N.** *Development and Characterization of Micro/Nanostructured Surfaces for Enhanced Condensation.* Massachusetts : Massachusetts Institute of Technology, 2013.

43. *Enhanced Jumping-Droplet Departure.* **Kim, M-K et al.** 49, 2015, Langmuir, Vol. 31, pp. 13452-13466.

44. **Chen, X et al.** *Coalescence-Induced Jumping of multiple Condensate Droplets on Hierarchical Superhydrophobic Surfaces.* s.l. : Scientific Reports, 2016.

45. **Miljkovic, N. et al.** *Jumping-Droplet Electrostatic Energy Harvesting.* s.l. : American Institute of Physics, 2014.

46. *A Comprehensive Model of Electric-Field-Enhanced Jumping-Droplet Condensation on Superhydrophobic Surfaces.* **Birbarah, P et al.** 28, 2015, Langmuir, Vol. 31, pp. 7885-7896.

47. *Hierarchical micro/nano structures for super-hydrophobic surfaces and super-lyophobic surface against liquid metal.* **Yong, Y. et al.** 2014, Micro and Nano Syst Lett.